

# Survey of Gravitationally lensed Objects in HSC Imaging (SuGOHI) – V. Group-to-cluster scale lens search from the HSC–SSP Survey

Anton T. Jaelani<sup>1,2,3</sup>★ Anupreeta More<sup>4,5</sup> Masamune Oguri,<sup>4,6,7</sup>  
Alessandro Sonnenfeld<sup>4,8</sup> Sherry H. Suyu,<sup>9,10,11</sup> Cristian E. Rusu<sup>12</sup>,  
Kenneth C. Wong<sup>4</sup> James H. H. Chan<sup>13</sup> Issha Kayo<sup>14</sup> Chien-Hsiu Lee<sup>15</sup>,  
Dani C.-Y. Chao,<sup>9,10</sup> Jean Coupon,<sup>16</sup> Kaiki T. Inoue<sup>1</sup> and Toshifumi Futamase<sup>17</sup>

*Affiliations are listed at the end of the paper*

Accepted 2020 April 16. Received 2020 March 29; in original form 2020 February 5

## ABSTRACT

We report the largest sample of candidate strong gravitational lenses belonging to the Survey of Gravitationally lensed Objects in HSC Imaging for group-to-cluster scale (SuGOHI-c) systems. These candidates are compiled from the S18A data release of the Hyper Suprime-Cam Subaru Strategic Program (HSC–SSP) Survey. We visually inspect  $\sim 39\,500$  galaxy clusters, selected from several catalogues, overlapping with the Wide, Deep, and UltraDeep fields, spanning the cluster redshift range of  $0.05 < z_{\text{cl}} < 1.38$ . We discover 641 candidate lens systems, of which 536 are new. From the full sample, 47 are almost certainly bona fide lenses, 181 of them are highly probable lenses, and 413 are possible lens systems. Additionally, we present 131 lens candidates at galaxy scale serendipitously discovered during the inspection. We obtained spectroscopic follow-up of 10 candidates using the X-shooter. With this follow-up, we confirm eight systems as strong gravitational lenses. Of the remaining two, one of the sources is too faint to detect any emission, and the other has a tentative redshift close to the lens redshift, but additional arcs in this system are yet to be observed spectroscopically. Since the HSC–SSP is an ongoing survey, we expect to find  $\sim 600$  definite or probable lenses using this procedure and even more if combined with other lens finding methods.

**Key words:** gravitational lensing: strong – methods: observational – surveys – galaxies: clusters: general.

## 1 INTRODUCTION

The standard model of cosmology suggests that the Universe is dominated by dark matter and dark energy. Strong gravitational lensing is a phenomenon where multiple-lensed images of distant sources can be seen due to deflection by the gravity of intervening massive objects such as galaxies and galaxy clusters. Gravitational lensing has been shown to be a promising technique to probe these dark components. Lensing has been used to study distant galaxies with extreme magnification (e.g. Swinbank et al. 2009; Zitrin & Broadhurst 2009; Richard et al. 2011), infer substructure in the lensing haloes (e.g. More et al. 2009; Vegetti, Czoske & Koopmans 2010a; Vegetti et al. 2010b; Hezaveh et al. 2016), constrain the Hubble constant (e.g. Suyu et al. 2010; Bonvin et al. 2017; Wong et al. 2019), and place constraints on the slope of the inner density profile of the lensing haloes (e.g. Koopmans & Treu

2003; Koopmans et al. 2006; More et al. 2008; Barnabè et al. 2009; Koopmans et al. 2009).

This has motivated dedicated efforts to search for gravitational lenses in large astronomical surveys e.g. the Hyper Suprime-Cam Subaru Strategic Program (HSC–SSP) Survey (Aihara et al. 2018a), DESI Legacy Imaging Surveys (Dey et al. 2019), Kilo Degree Survey (KiDS, de Jong et al. 2015), and Dark Energy Survey (DES, Dark Energy Survey Collaboration 2016). Specifically, large imaging and spectroscopic surveys have allowed inferences of statistical properties of lenses such as constraints on the stellar initial mass function (e.g. Ferreras et al. 2010; Treu et al. 2010; Sonnenfeld et al. 2012, 2019), estimation of the fraction of dark matter in galaxy-scale haloes (e.g. Gavazzi et al. 2007; Grillo 2010; Faure et al. 2011; More et al. 2011; Ruff et al. 2011), and even constraints on cosmology (e.g. Gladders et al. 2003; Oguri et al. 2012).

As mentioned above, most of the surveys have primarily focused on studying galaxy-scale or cluster-scale structures. As a result, the matter distribution in galaxies and galaxy clusters is relatively well

\* E-mail: anton@phys.kindai.ac.jp

studied via both strong and weak lensing. A further improvement in our understanding has come from the use of complementary methods to lensing such as stellar kinematics, satellite kinematics, and X-ray scaling relations. In contrast, there has not been much progress (in the last decade) on mass distributions of galaxy groups in the mass range of  $10^{12}$ – $10^{14} M_{\odot}$ , intermediate to galaxies and galaxy clusters. Using X-ray samples to study the intra-group medium at low redshifts (Helsdon & Ponman 2000), mass-to-light ratios of groups from the Canadian Network for Observational Cosmology 2 (CNO2) sample (e.g. Parker et al. 2005), the faint end of the luminosity function of nearby compact groups (e.g. Krusch et al. 2006), the concentration–mass ( $c - M$ ) relation of groups (e.g. Mandelbaum, Seljak & Hirata 2008; Newman, Ellis & Treu 2015), colours and star formation of galaxy groups (e.g. Balogh et al. 2009, 2011), scaling relations of X-ray selected groups (Rines & Diaferio 2010), and baryon fractions from the Two Micron All Sky Survey (2MASS) (Dai et al. 2010) are some examples of investigations of galaxy groups.

We still do not have a detailed understanding of the matter distribution, formation, and evolution of galaxy groups. Being one of the important components in the hierarchical assembly of structures in the Universe, galaxy groups are much more massive than galaxy-scale haloes and are concentrated enough to act as lenses. Furthermore, since galaxy groups are quite abundant compared to massive structures like galaxy clusters, the probability of finding group-scale lenses is also large. Hence, strong lensing can be successfully used to study group-scale haloes (Limousin et al. 2009; More et al. 2012; Foëx et al. 2013, 2014; Verdugo et al. 2014; Newman et al. 2015).

In this work, we conduct a systematic search of group- and cluster-scale lenses as part of the Survey of Gravitationally lensed Objects in HSC Imaging (SuGOHI) and also present the results of spectroscopic follow-up of a sub-sample of these systems. The galaxy-scale lens sample (SuGOHI-g) is presented in Sonnenfeld et al. (2018), Sonnenfeld et al. (2019), and Wong et al. (2018), and the results of a search for lensed quasars (SuGOHI-q) are reported in Chan et al. (2020). This paper is organized as follows. In Section 2, we describe the HSC–SSP imaging data used in our search. In Section 3, we describe the procedure for finding new strong gravitational lens systems. We present our newly discovered lens candidates in Section 4. In Section 5, we describe our spectroscopic follow-up observation. We present our summary and conclusion in Section 6.

## 2 THE DATA

The Subaru Strategic Program (SSP) survey is carried out with the Hyper Suprime-Cam (HSC, Coupon et al. 2018; Furusawa et al. 2018; Huang et al. 2018; Kawanomoto et al. 2018; Komiyama et al. 2018; Miyazaki et al. 2018), a  $1.7 \text{ deg}^2$  field-of-view optical camera recently installed on the 8.2-m *Subaru telescope*. The HSC–SSP Survey has three fields: the Wide field is expected to cover a  $1400 \text{ deg}^2$  area in five bands ( $g$ ,  $r$ ,  $i$ ,  $z$ , and  $y$ ) to an  $i$ -band depth of 26.2 by its completion, while the Deep+UltraDeep fields are expected to cover smaller areas of about  $27 \text{ deg}^2$  and  $3.5 \text{ deg}^2$ , respectively [see Aihara et al. (2018a) for more details about the survey]. We use the photometric data from the S18A data release, which covers  $1114 \text{ deg}^2$  (out of which  $305 \text{ deg}^2$  is full depth) in Wide and  $31 \text{ deg}^2$  in Deep+UltraDeep, at least in one filter and one exposure (Aihara et al. 2019). The data are processed with the reduction pipeline HSCPIPE v6.7 (Bosch et al. 2018), a version of the Large Synoptic Survey Telescope stack (Axelrod et al. 2010;

Jurić et al. 2017; Ivezić et al. 2008, 2019). The median seeing of S18A data is 0.61 arcsec in the  $i$  band, 0.85 arcsec in the  $g$  band, and the pixel scale of HSC is 0.168 arcsec.

The redshifts used in this work are obtained from the photometric redshift catalogue of the HSC–SSP Survey, determined using the Direct Empirical Photometric code (DEmP, Hsieh & Yee 2014). The HSC–SSP photometric redshifts are most accurate at  $0.2 \lesssim z_{\text{phot}} \lesssim 1.5$ . The point estimates of the photometric redshift are accurate to better than 1 per cent in terms of  $\langle \Delta z / (1 + z) \rangle$  with a scatter of  $\approx 0.04$  and an outlier rate of  $\approx 8$  per cent for galaxies with  $i < 24$  mag. A more detailed description of DEmP’s application to the HSC–SSP data is presented in Tanaka et al. (2018). Since the HSC–SSP Survey footprint has some overlap with that of the Sloan Digital Sky Survey (SDSS), we also extracted spectroscopic redshifts, whenever available, from the SDSS Data Release 15 (Aguado et al. 2019) catalogues.

## 3 LENS CANDIDATE SELECTION

In this section, we describe how the cluster catalogues are selected for visual inspection and our criteria to grade the lens candidates. Visual inspection of cluster catalogues is still a practically useful method for lens finding at group/cluster scales because it allows for selection of candidates with rich diversity and complexity while maintaining high purity. We used the HSCMAP (SKY EXPLORER),<sup>1</sup> an online tool, to visually inspect colour images of the clusters (see Section 3.1). The lens search relied on morphology and colour information to visually analyse properties of the lensed images and the galaxies in the cluster to assess the plausibility of lensing. Inspectors could control the spatial scales, contrast, and brightness, and could choose different combinations of the HSC filters.

### 3.1 Parent catalogues

We used galaxy cluster catalogues within the footprint covering the HSC–SSP S18A imaging. The on-sky distribution of these clusters, along with survey footprints, is shown in Fig. 1. We also give the number of clusters detected from each of the four catalogues in Table 1.

#### 3.1.1 Clusters from the HSC–SSP Survey

Our primary cluster catalogue is called CAMIRA, which is produced by running the cluster-finding algorithm (Oguri 2014) on the internal HSC–SSP data release S18A<sup>2</sup> (Aihara et al. 2019), covering roughly  $465 \text{ deg}^2$  and  $28 \text{ deg}^2$ , in all five filters, for Wide and Deep+UltraDeep fields, respectively. The CAMIRA is validated through comparisons with existing spectroscopic and X-ray data as well as mock galaxy catalogues.

We obtain 14 992 clusters, comprising of 14 350 clusters from the Wide fields and 642 clusters from the Deep fields, with the richness limit  $N_{\text{ric,CAMIRA}} > 10$  spanning a redshift range of  $0.1 < z_{\text{cl}} < 1.38$ . Richness in CAMIRA is defined to be the number of red member galaxies with stellar mass  $M_{\text{star}} \geq 10^{10.2} M_{\odot}$  lying within a physical radius of  $\approx 1.4 \text{ Mpc}$ . The richness limit  $N_{\text{ric,CAMIRA}} = 10$  corresponds

<sup>1</sup><https://hsc-release.mtk.nao.ac.jp/hscMap-pdr2/app/>, similar tool but for public data release 2.

<sup>2</sup>Note that the currently published CAMIRA catalogue makes use of the data release S16A only and it can be obtained from Oguri et al. (2018). However, this is a subsample of the catalogue used in our study.

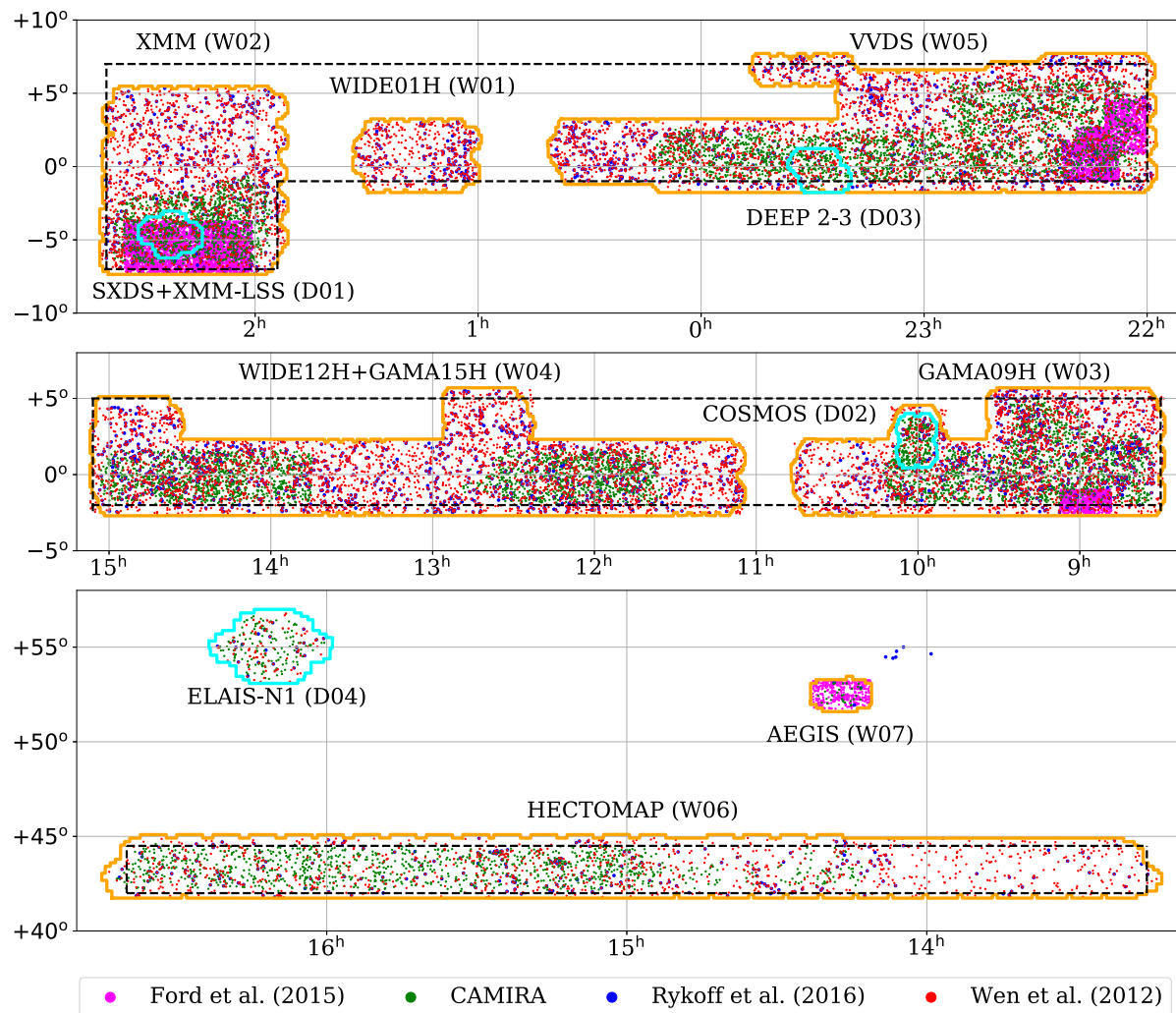


**Figure 1.** The Hyper Suprime-Cam Subaru Strategic Program (HSC–SSP) observational footprint shown in equatorial coordinates. The orange and cyan boxes indicate the Wide and Deep+UltraDeep fields for the S18A data release (internal). The dashed black boxes indicate the approximate boundaries of the three disjoint regions that will make up the final Wide survey. The overlapping cluster catalogues are shown by different point colours.

**Table 1.** Clusters found in the HSC–SSP S18A footprint from different algorithms, some of which are external to the HSC Survey collaboration.

Catalogue	Catalogue label	Number of clusters
CAMIRA	CAM	14 992
Ford et al. (2015)	F	9475
Rykoff et al. (2016)	R	2968
Wen, Han & Liu (2012)	W	12 000

to  $M_{200} \approx 7 \times 10^{13} M_\odot$ , where  $M_{200}$  is the cluster mass within  $r_{200}$ , by extrapolating the richness-mass relation of CAMIRA from Murata et al. (2019).  $r_{200}$  is the radius within which the mean density of a cluster is 200 times the critical density of the Universe. The cluster sample is shown by green points in Fig. 1. The CAMIRA cluster catalogue is still being constructed from the HSC–SSP Survey data, since the HSC survey is an ongoing and several patches are likely to have incomplete imaging data, e.g. has  $\leq 4$  filters. As a result, we decided to make use of other public catalogues constructed from previous surveys that have overlapped with the HSC–SSP Survey footprint, e.g. the SDSS (York et al. 2000) and the Canada-

France Hawaii Telescope Lensing Survey (CFHTLenS, Heymans et al. 2012). Also, including more cluster catalogues maximizes the chance of finding more group-to-cluster scale lenses.

### 3.1.2 Clusters from data release 8 of SDSS-III data

The HSC–SSP Survey footprint has almost complete overlap with SDSS footprint. We thus have two extensive cluster catalogues, Wen et al. (2012) and Rykoff et al. (2016), that can be used. Both catalogues are derived from the galaxy data of  $14\,000 \text{ deg}^2$  of SDSS-III (Eisenstein et al. 2011). Wen et al. (2012) identified 132 684 clusters (12 000 of them overlap with the HSC–SSP S18A footprint, see Table 1 and red points in Fig. 1) in the redshift range of  $0.05 \leq z_{\text{cl}} < 0.8$ . The clusters are selected if their richness  $N_{\text{ric}, \text{Wen}} \geq 12$ , which corresponds to  $M_{200} \approx 0.6 \times 10^{14} M_\odot$  and a number of member galaxies candidates  $N_{200} \geq 8$  within  $r_{200}$ . We also used clusters from the red-sequence Matched-filter Probabilistic Percolation (REDMAPPER, for the details see Rykoff et al. 2014) cluster finding algorithm (version 6.3). This catalogue has a total of 25 236 clusters (2 968 are overlapping with the HSC–SSP S18A footprint, see Table 1 and blue points in Fig. 1) in the redshift range

of  $0.08 \leq z_{\text{cl}} < 0.55$  with  $N_{\text{ric, REDMAPPER}} \geq 20$ , which corresponds to  $M_{200} \gtrsim 10^{14} M_{\odot}$ . For more detailed description of the catalogue, see Rykoff et al. (2016).

### 3.1.3 CFHTLenS data

Ford et al. (2015) have a sample of 18 056 clusters (9475 of them overlap with the HSC–SSP S18A footprint, see Table 1) at redshifts  $0.2 \leq z_{\text{cl}} \leq 0.9$ . The clusters have been detected using the 3D-Matched-Filter Galaxy Cluster Finder in the  $\sim 154 \text{ deg}^2$  CFHTLenS survey (Milkeraitis et al. 2010; Ford et al. 2014) with a significance  $\geq 3.5$  and richness  $N_{\text{ric, Ford}} > 2$ , which corresponds to  $M_{200} \approx 6 \times 10^{12} M_{\odot}$ . This field has a substantial overlap with the S18A data (see magenta points in Fig. 1).

## 3.2 Ranking criteria

We identified 39 435 clusters, located in the HSC–SSP S18A footprint, from the four catalogues combined. Inspectors use the online HSCMAP (SKY EXPLORER)<sup>1</sup> server to inspect colour images of the clusters (Aihara et al. 2018b, 2019). In the first step, we divided the clusters into three redshift bins, which were inspected by three inspectors per redshift bin. After we compiled the 1160 candidates from all redshift bins combined, nine inspectors independently assigned a rank from 0 to 3, according to the following criteria:

- 3: almost certainly a lens,
- 2: probably a lens,
- 1: possibly a lens, and
- 0: not a lens.

We further refined the sample of candidates by applying the following scheme:

- A:  $\langle \text{Rank} \rangle > 2.5$ ,
- B:  $1.5 < \langle \text{Rank} \rangle \leq 2.5$ ,
- C:  $0.5 < \langle \text{Rank} \rangle \leq 1.5$ , and
- Not a lens:  $\langle \text{Rank} \rangle \leq 0.5$

where  $\langle \text{Rank} \rangle$  is the mean rank given by individual inspectors. The final sample, thus, consists of 772 candidates. Systems with highly discrepant ranks were discussed and regraded to mitigate such discrepancies.

## 4 RESULTS

The Einstein radius,  $\theta_{\text{Eins}}$ , is the best parameter to represent mass of the lens, which can be approximated from the arc radius,  $R_{\text{arc}} \approx 2\theta_{\text{Eins}}$  (More et al. 2012). Typically, lensing haloes with  $\theta_{\text{Eins}} \geq 2$  arcsec are very massive lenses with significant contribution from the environment of the primary lensing galaxy (Oguri 2006; More et al. 2012). Here, we calculated the arc radius by assuming a circle roughly covering the candidate arc centred on the brightest cluster galaxy (BCG).

Next, we separated the graded systems into two groups: SuGOHI-c and additional lenses at galaxy scale (SuGOHI-g, see Appendix A), which are shown by Tables 3 and A2, respectively. The classification criteria for a candidate to be included in SuGOHI-c are the following:

1. If the lensing is due to the BCG (see the panel a in Fig. 2), and
2. either the angular separation of the arc from the lens centre, the arc radius,  $R_{\text{arc}} \geq 2$  arcsec (e.g. HSC J1557+4206),

3. or if the lensing is caused by more than one galaxy enclosed by a ring through the arc or multiple images (e.g. HSC J2228+0022).

If none of the above are satisfied, candidates fall in the SuGOHI-g sample as being serendipitously discovered during the inspection [e.g. HSC J0904+0102 (Jaelani et al. 2020)], which is at a similar position to HSC J1414–0136 with respect to the cluster but has  $R_{\text{arc}} < 2$  arcsec; see the panel c of Fig. 2] and are reported in the Appendix.

For the first classification criteria, if a BCG is misclassified<sup>3</sup> as a member galaxy by the algorithm, only then do we accept it as a SuGOHI-c system. A member galaxy may be aided by the group potential, but then the arc separation also needs to be  $R_{\text{arc}} \geq 2$  arcsec (see the middle panel in Fig. 2). Otherwise, this could still be a galaxy-scale lens. In some rare cases, an arc radius cannot be quantified because it is being deflected by multiple galaxies on either side (e.g. see HSC J0209–0448, grade C in the online material<sup>4</sup>). These are also included as SuGOHI-c.

A total of 641 systems (including 536 new lenses presented for the first time) are in the SuGOHI-c sample. These consist of 47 Grade A, 181 Grade B, and 413 Grade C systems, respectively. We found some candidate systems in more than one catalogue that are shown in Fig. 3. The CAMIRA produces the largest number of candidate systems. We also found many candidates serendipitously that were missed by the parent cluster catalogues. Some of these lenses were also discovered independently by the citizen science project (SPACE WARPS, Marshall et al. 2016; More et al. 2016) from the HSC–SSP Survey (see details in Sonnenfeld et al. 2020). We present the lens candidate statistics in Table 2.

We provide the full candidate systems of the SuGOHI-c in the online material<sup>3</sup>. The list of SuGOHI-c with grades A and B is presented in Table 3, which provides the system name, the equatorial coordinates, the lens and source redshift, the arc radius, the mean and the  $\sigma$  of the rank, a qualitative grade, the parent catalogue, and references from previous studies. Fig. 4 show composite colour ( $gri$  or  $riz$ ) cutouts of grades A and B for the SuGOHI-c sample. At the top of each cutout is the system name. At the bottom left is a grade (labelled 'A' or 'B'), as well as a label 'C', 'D', or 'K' if the lens is spectroscopically confirmed, previously discovered, and well-known, respectively. The known candidates have been identified by cross-matching with the published systems in the literature, as reported in Table 3.

We show the photometric redshift distribution of lens galaxies and arc radii of the systems in Fig. 5, and for comparison, we also show 125 lens systems of the Strong Lensing Legacy Survey - ARCS (SARCS) sample distribution with  $R_{\text{arc}} \geq 2$  arcsec from More et al. (2012). We find that the mean lens redshifts for the SuGOHI-c sample and SARCS sample are  $z = 0.50 \pm 0.23$  and  $z = 0.58 \pm 0.22$ , respectively. We note that the mean redshifts of both samples have good agreement. We find that the peak of the SuGOHI-c lens sample, on the other hand, is at  $z \sim 0.3$ –0.4, which is consistent with the peak expected from numerical simulation (Bartelmann et al. 1998).

During our inspection, we also found a number of strong lens systems with red-coloured sources (e.g. HSC J0211–0343, HSC J1143+0102). We mark such systems with a † in Table 3. Some of them are high redshift galaxies at  $z \sim 6$  (Oguri et al., in preparation,

<sup>3</sup>A BCG is considered to be misclassified if it is visually much brighter than its neighbours and/or the galaxy labelled as BCG by the cluster-finding algorithm.

<sup>4</sup><http://www-utap.phys.s.u-tokyo.ac.jp/~oguri/sugohi/>

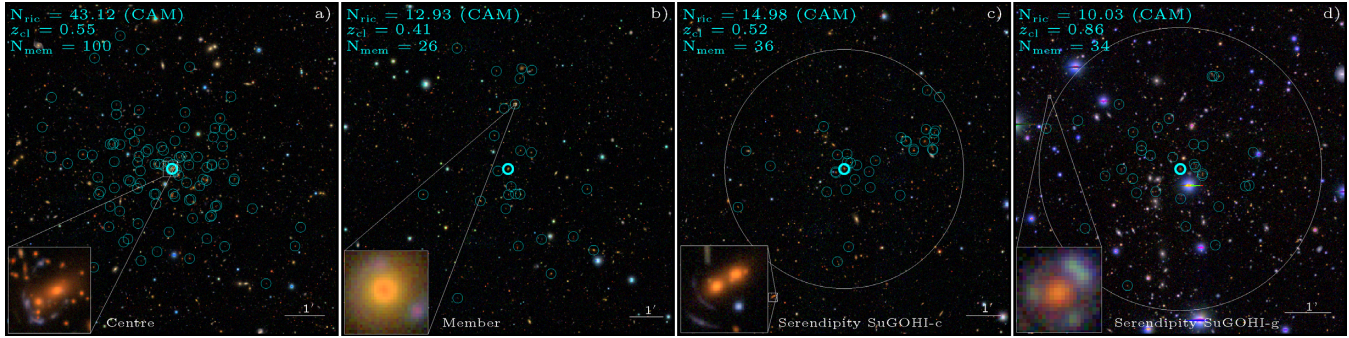


**Figure 2.** Types of lens candidates depending on their location with respect to galaxy clusters. Lens candidates where the BCG acts as a lens (**panel a**, e.g. HSC J1441–0053) or a member galaxy (see more description in Section 4) acts as a lens (**panel b**, e.g. HSC J1234–0009) are classified as SuGOHI-g, otherwise as serendipitous discoveries (**panels c and d**, e.g. HSC J1414–0136 and HSC J0904+0102, for SuGOHI-c and -g, respectively). The cyan circles indicate member galaxies of a cluster and the brightest cluster galaxy (BCG) is indicated by a thicker circle. The white circle indicates the region that encloses member galaxies with the BCG at the centre. The richness  $N_{\text{ric}}$ , cluster redshift  $z_{\text{cl}}$ , and number of galaxy member  $N_{\text{mem}}$  are shown at the top left.

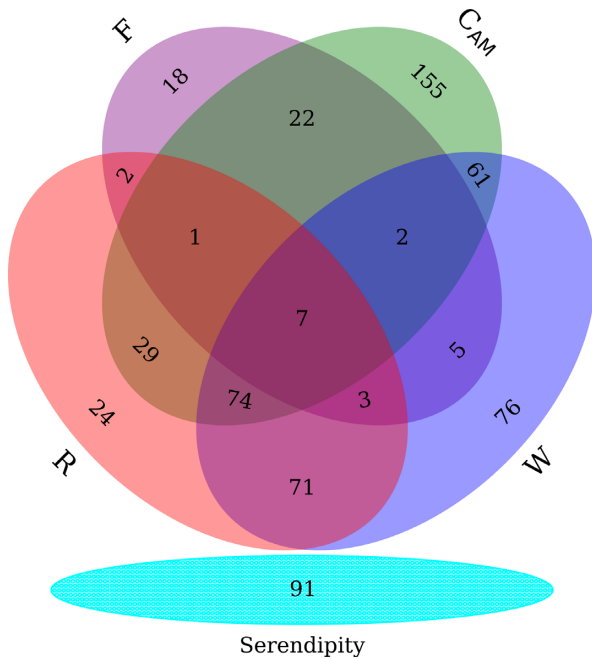


**Figure 3.** Distribution of lens candidates according to the parent cluster catalogues. The letters represent the parent cluster catalogues as presented in Table 1. The Venn diagram is divided into two panels: 550 lens systems of SuGOHI-c correspond to the parent cluster (upper) and 91 lens systems that are serendipitously (bottom) discovered during the inspection and, thus, are not listed as BCGs of the clusters or members with  $R_{\text{arc}} \geq 2$  arcsec.

**Table 2.** Lens candidate statistics. 'CAM F R W' represent the parent cluster catalogues as presented in Table 1.

	Grade			Total	Previously known / spectroscopically confirmed
	A	B	C		
SuGOHI-c	47	181	413	641	105
CAM	21	128	202	351	68
F	5	15	40	60	20
R	20	56	136	212	40
W	26	79	194	299	58
Serendipity	6	24	61	91	12

and Ono et al., in preparation). We further note that HSC J2211–0008 has a spectroscopically confirmed lensed source, which is a Lyman-break galaxy at  $z = 2.26$ . Details of the follow-up Subaru observations and analysis of this system will be reported in More et al. (in preparation).

## 5 SPECTROSCOPIC FOLLOW-UP

We carried out spectroscopic observations of 10 candidates from SuGOHI-c sample in order to confirm the lensing nature and obtain spectroscopic redshifts essential for detailed mass modelling of strong lenses (Jaelani et al., in preparation). Our sample was part of the larger spectroscopic campaign for SuGOHI lenses (ESO programme 099.A-0220, PI: S. Suyu) with the Very Large Telescope (VLT)'s X-shooter. These candidates were selected from an early sample of grade A-B lenses with  $z_{\ell} > 0.6$  from a smaller footprint. X-shooter is an Echelle spectrograph (Vernet et al. 2011), with an allowed wavelength range of  $\lambda\lambda 3000–25\,000$  Å. The spectra are acquired through three arms, the ultraviolet (UVB,  $\lambda\lambda 3000–5500$  Å), the visual (VIS,  $\lambda\lambda 5000–10\,500$  Å), and the near-infrared (NIR,  $\lambda\lambda 10\,000–25\,000$  Å). The lensed sources were observed using slit widths of 1.0, 0.9, and 0.9 arcsec in the UVB, VIS, and NIR arms, respectively, with a binning of  $2 \times 2$  applied to the UVB and VIS data. We set the position angle (PA) of the long slit to be preferentially along the lensed arc (see Fig. 6). In order to optimize sky background subtraction, we dithered the observations in the standard ABBA nodding pattern.

Each system was observed in slit mode during either one (e.g. HSC J0224–0336) or two (e.g. HSC J1202+0039) observation blocks (OBs) to reach the optimal signal-to-noise ratio. Each OB corresponds to roughly 1 h of telescope time and consists of  $10 \times 285$  s exposures obtained in an ABBA nodding pattern to optimize background subtraction in the NIR arm. Exposure times in the UVB and VIS arms are slightly shorter due to the longer readout time. Observations were executed with seeing full width at half-maximum  $<0.9$  arcsec on target position. Initially, we reduce the spectroscopic data using the ESO REFLEX software (version 2.9.0) combined with X-shooter pipeline recipes (v3.1.0) (Modigliani et al. 2010; Freudling et al. 2013). The pipeline recipes perform standard bias subtraction and flat-fielding of the raw spectra. Cosmic rays are removed using LACOSMIC (van Dokkum 2001). For each arm, we extract the orders and rectify them in wavelength space using a wavelength solution previously obtained from the calibration

**Table 3.** SuGOHI-c candidates, with grades A and B, selected by visual inspection of galaxy cluster catalogues. Redshifts are DEmP photometric and SDSS DR15 spectroscopic redshifts. PC indicates the parent cluster catalogue through which a candidate was selected as in Table 1. Systems with †, X, C, D, and K are the lens candidates that have red-coloured sources, X-shooter follow-up, spectroscopically confirmed, previously discovered, and known, respectively. Systems with references are previously known, whereas other objects with '...' are new.

Name	$\alpha$ (J2000)	$\delta$ (J2000)	$z_{\ell,\text{phot}}$	$z_{\ell,\text{spec}}$	$R_{\text{arc}}$ (arcsec)	Rank	$\sigma_{\text{Rank}}$	Grade	PC	References
HSC J0003+0054	0.8045	0.9069	1.13	...	3.22	1.78	0.63	B	CAM	...
HSC J0004–0103 <sup>C</sup>	1.2155	–1.0551	0.48	...	3.23	2.78	0.42	A	...	1, 15
HSC J0008+0015	2.2032	0.2641	0.40	0.397	2.57	2.75	0.46	A	...	...
HSC J0014–0057	3.7257	–0.9525	0.55	0.535	13.79	2.25	0.46	B	W	...
HSC J0032+0100	8.0733	1.0102	0.37	0.390	6.48	2.88	0.35	A	RW	...
HSC J0034+0225 <sup>C</sup>	8.6173	2.4227	0.32	...	13.01	2.75	0.46	A	RW	15
HSC J0107+0117† <sup>D</sup>	16.7886	1.2918	0.44	0.422	9.64	2.00	0.47	B	W	2
HSC J0112–0022	18.1073	–0.3798	0.50	0.466	2.09	1.75	0.46	B	...	...
HSC J0156–0424	29.2265	–4.4071	0.12	...	3.03	2.44	0.50	B	CAMRW	...
HSC J0157–0515	29.3186	–5.2537	0.53	0.560	2.98	2.29	0.45	B	CAM	...
HSC J0159–0358	29.9093	–3.9829	1.11	...	4.38	2.29	0.45	B	CAM	...
HSC J0208–0237	32.0673	–2.6233	0.53	0.514	7.41	2.14	0.83	B	CAMRW	...
HSC J0209–0643 <sup>D</sup>	32.3721	–6.7200	0.40	0.407	3.08	2.67	0.67	A	FW	3, 7
HSC J0210–0038	32.6662	–0.6422	0.24	0.287	5.72	1.63	0.74	B	RW	...
HSC J0211–0343†	32.8150	–3.7299	0.75	...	3.98	3.00	0.00	A	CAMF	...
HSC J0214–0206 <sup>D</sup>	33.5333	–2.1081	0.67	...	3.00	2.11	0.74	B	...	3
HSC J0214–0535 <sup>K</sup>	33.5335	–5.5925	0.47	0.445	6.37	2.86	0.35	A	CAMFRW	7, 9, 18
HSC J0217+0033	34.3360	0.5536	0.36	0.381	5.04	1.88	0.84	B	RW	...
HSC J0218–0515 <sup>D</sup>	34.5306	–5.2601	0.56	0.649	2.61	1.57	0.90	B	CAM	7, 9
HSC J0219–0527 <sup>D</sup>	34.9850	–5.4665	0.29	0.285	3.00	2.44	0.73	B	CAMFW	7, 9
HSC J0220–0222 <sup>D</sup>	35.1766	–2.3668	0.60	0.546	3.99	2.14	0.64	B	CAM	5
HSC J0222–0222	35.5932	–2.3699	1.18	...	3.18	1.67	0.67	B	CAM	...
HSC J0222–0258	35.7480	–2.9743	0.46	...	2.12	1.57	0.50	B	CAM	...
HSC J0224–0346 <sup>D</sup>	36.0040	–3.7738	0.95	...	2.56	1.86	0.64	B	CAM	7
HSC J0224–0336 <sup>X C</sup>	36.0437	–3.6015	0.61	0.613	3.89	2.29	0.45	B	CAMW	5
HSC J0225–0532 <sup>D</sup>	36.3888	–5.5346	0.58	0.566	3.98	1.56	0.73	B	CAMF	8
HSC J0228–0212	37.0118	–2.2005	0.23	0.206	3.76	2.29	0.45	B	CAMRW	...
HSC J0230–0540 <sup>D</sup>	37.5355	–5.6774	0.46	0.498	2.26	1.57	0.50	B	CAMF	8
HSC J0230–0159	37.7006	–1.9841	1.10	...	4.50	1.56	0.68	B	CAM	...
HSC J0231–0621	37.7516	–6.3612	1.17	...	2.18	3.00	0.00	A	CAM	...
HSC J0232–0323 <sup>K</sup>	38.2078	–3.3905	0.46	0.450	3.77	3.00	0.00	A	CAM	1, 2, 3, 10
HSC J0233–0228	38.2734	–2.4769	0.61	0.572	4.99	2.71	0.45	A	CAM	...
HSC J0233–0328	38.3837	–3.4671	1.12	...	4.17	1.71	1.03	B	CAM	...
HSC J0235–0634 <sup>D</sup>	38.9092	–6.5684	0.20	0.181	2.13	2.00	0.00	B	CAMW	5
HSC J0236–0332 <sup>D</sup>	39.1554	–3.5389	0.28	0.269	2.12	3.00	0.00	A	CAMRW	5
HSC J0238–0348	39.5988	–3.8036	0.29	0.322	4.29	1.63	0.52	B	RW	...
HSC J0239–0127 <sup>D</sup>	39.9260	–1.4632	0.35	...	4.26	2.33	0.47	B	...	2
HSC J0239–0134 <sup>K</sup>	39.9714	–1.5827	0.37	0.373	10.86	2.88	0.35	A	RW	3, 14
HSC J0837+0156 <sup>D</sup>	129.3593	1.9441	0.39	0.396	2.67	2.29	0.45	B	CAMR	4, 5
HSC J0838+0208	129.7372	2.1474	0.36	0.360	6.95	1.56	0.54	B	CAMRW	...
HSC J0839–0140†	129.8890	–1.6792	0.28	...	2.43	2.56	0.68	A	W	...
HSC J0839+0228	129.9141	2.4756	0.42	0.431	3.87	1.56	0.68	B	CAM	...
HSC J0840+0135	130.2476	1.5970	0.56	0.550	3.42	1.56	0.50	B	CAMR	...
HSC J0844–0010	131.1135	–0.1832	0.37	...	4.62	1.56	0.50	B	CAMRW	...
HSC J0845–0054 <sup>D</sup>	131.3341	–0.9156	0.41	...	7.70	1.71	0.70	B	CAMRW	4
HSC J0846–0154	131.6363	–1.9049	1.03	...	3.93	1.67	0.67	B	CAM	...
HSC J0846+0446 <sup>K</sup>	131.6978	4.7679	0.23	0.241	4.41	1.75	0.71	B	RW	10, 19
HSC J0852+0025	133.1269	0.4203	0.29	...	9.26	2.29	0.70	B	R	...
HSC J0854–0121 <sup>K</sup>	133.6944	–1.3607	0.34	...	5.02	2.88	0.35	A	FRW	4, 9, 18
HSC J0855+0024	133.9344	0.4105	0.56	...	3.45	1.57	0.50	B	CAMRW	...
HSC J0856+0125 <sup>D</sup>	134.0864	1.4174	0.68	0.719	2.60	2.29	0.70	B	CAM	5
HSC J0904+0125 <sup>X C</sup>	136.0180	1.4208	0.91	...	5.20	2.29	0.45	B	CAM	...
HSC J0904+0426	136.1276	4.4466	0.32	0.457	4.54	3.00	0.00	A	W	...
HSC J0906+0119	136.5461	1.3308	0.65	0.605	3.82	1.67	0.47	B	...	...
HSC J0907+0057 <sup>X C</sup>	136.9767	0.9587	0.72	...	7.00	2.29	0.70	B	CAM	...
HSC J0908+0119	137.0261	1.3319	0.69	0.659	5.08	1.67	0.47	B	CAMW	...
HSC J0909+0405	137.2978	4.0883	0.81	...	2.41	1.57	0.50	B	CAM	...
HSC J0912+0415	138.1252	4.2654	0.44	0.453	2.26	1.56	0.68	B	CAMW	...

**Table 3** – *continued*

Name	$\alpha$ (J2000)	$\delta$ (J2000)	$z_{\ell,\text{phot}}$	$z_{\ell,\text{spec}}$	$R_{\text{arc}}$ (arcsec)	Rank	$\sigma_{\text{Rank}}$	Grade	PC	References
HSC J0913+0352†	138.3040	3.8705	0.47	0.456	2.37	1.57	0.90	B	CAMR	...
HSC J0919+0336 <sup>D</sup>	139.7692	3.6107	0.45	0.444	2.15	3.00	0.00	A	CAMRW	5
HSC J0921+0214 <sup>D</sup>	140.4025	2.2363	0.33	0.319	2.15	2.29	0.45	B	CAMW	4
HSC J0922+0259	140.6465	2.9950	1.10	...	2.15	2.33	0.50	B	CAM	...
HSC J0925+0226	141.2609	2.4362	0.39	0.390	4.66	1.89	0.87	B	CAMW	...
HSC J0926+0500	141.6992	5.0005	0.49	0.462	2.68	1.88	0.64	B	RW	...
HSC J0935+0047	143.8137	0.7959	0.37	0.358	7.82	2.38	0.92	B	CAMR	...
HSC J0943–0154	145.8653	–1.9149	0.44	0.450	2.42	1.56	0.50	B	CAM	...
HSC J0943+0059 <sup>D</sup>	145.9510	0.9903	0.43	...	2.43	3.00	0.00	A	CAMR	2
HSC J0947–0111†	146.8682	–1.1925	0.26	0.239	4.08	2.00	0.47	B	CAMW	...
HSC J0951–0014	147.9171	–0.2391	0.37	0.421	14.13	1.63	0.52	B	CAMRW	...
HSC J0958+0109	149.6311	1.1603	0.57	0.550	2.72	2.11	0.60	B	CAM	...
HSC J0959+0101	149.8211	1.0329	0.45	0.446	3.08	1.67	0.47	B	CAMRW	...
HSC J0959+0219 <sup>D</sup>	149.9833	2.3169	0.97	...	2.74	2.56	0.50	A	CAM	7
HSC J1005–0100	151.3869	–1.0078	0.40	0.420	6.19	1.67	0.47	B	CAMW	...
HSC J1005–0103	151.4756	–1.0660	1.05	...	3.97	1.56	0.68	B	CAM	...
HSC J1007–0123†	151.8009	–1.3879	0.93	...	2.19	1.56	0.83	B	...	...
HSC J1018–0121 <sup>D</sup>	154.6972	–1.3591	0.39	0.388	3.21	2.88	0.35	A	RW	2
HSC J1039–0216 <sup>D</sup>	159.7807	–2.2750	0.16	...	2.05	2.11	0.74	B	W	4
HSC J1139–0218	174.8726	–2.3071	0.79	...	3.52	2.78	0.42	A	W	...
HSC J1143–0047	175.7553	–0.7867	0.28	...	2.61	1.75	0.46	B	CAMRW	...
HSC J1143–0144 <sup>D</sup>	175.8743	–1.7418	0.11	0.106	2.56	3.00	0.00	A	RW	4, 12
HSC J1143+0013†	175.9262	0.2278	0.65	0.650	5.17	2.29	0.70	B	CAM	...
HSC J1144–0025	176.1623	–0.4299	0.73	0.614	2.23	2.00	0.76	B	CAMW	...
HSC J1147+0119	176.7731	1.3192	0.63	0.636	3.88	1.86	0.83	B	...	...
HSC J1147–0013 <sup>X C</sup>	176.9383	–0.2307	0.81	...	3.31	2.29	0.45	B	...	...
HSC J1152+0031 <sup>D</sup>	178.0592	0.5239	0.46	0.466	5.43	2.71	0.45	A	CAMW	4, 5
HSC J1153–0144	178.3794	–1.7363	0.11	...	24.60	2.13	0.00	B	CAMRW	...
HSC J1155+0053 <sup>D</sup>	178.8366	0.8843	0.31	0.283	3.65	1.71	0.45	B	...	4
HSC J1156–0019	179.0414	–0.3257	0.27	0.260	4.61	1.57	0.50	B	CAMR	...
HSC J1156–0021	179.0451	–0.3501	0.26	0.256	8.01	1.86	0.35	B	CAMRW	...
HSC J1156–0101 <sup>D</sup>	179.0548	–1.0339	0.44	...	4.60	1.57	0.50	B	CAM	4
HSC J1156–0037 <sup>X C</sup>	179.2234	–0.6316	0.92	...	3.86	1.71	1.03	B	CAM	...
HSC J1201+0126 <sup>X C</sup>	180.2978	1.4433	0.62	...	6.77	2.29	0.45	B	CAM	4
HSC J1201+0025	180.4603	0.4222	0.88	...	1.86	1.67	0.71	B	CAM	...
HSC J1202+0039 <sup>X C</sup>	180.7370	0.6584	0.70	0.689	4.18	2.29	0.45	B	CAM	...
HSC J1207–0103 <sup>D</sup>	181.9302	–1.0654	0.18	0.180	2.21	2.44	0.50	B	CAMW	4
HSC J1208+0128	182.2052	1.4791	0.71	...	2.20	2.22	0.42	B	CAM	...
HSC J1208–0103	182.2306	–1.0512	0.71	0.662	4.73	2.43	0.50	B	CAMW	...
HSC J1210–0112 <sup>D</sup>	182.5947	–1.2001	0.59	0.574	4.05	2.14	0.35	B	CAM	4
HSC J1211+0020	182.9875	0.3482	0.79	...	2.72	1.56	0.50	B	CAM	...
HSC J1222–0127	185.6074	–1.4485	0.29	0.295	10.76	2.78	0.42	A	W	...
HSC J1223–0210	185.8964	–2.1754	0.35	0.439	4.39	1.89	0.57	B	RW	...
HSC J1224–0042 <sup>D</sup>	186.2094	–0.7044	0.40	0.403	2.41	2.56	0.50	A	CAMR	4
HSC J1231+0023	187.7810	0.3921	0.60	0.591	5.94	1.89	0.87	B	CAMW	...
HSC J1231+0301	187.8949	3.0313	0.42	0.461	6.18	1.78	0.63	B	W	...
HSC J1233–0144	188.2623	–1.7352	0.63	...	9.72	2.00	0.67	B	CAM	...
HSC J1233+0131 <sup>D</sup>	188.2803	1.5300	0.42	0.425	3.39	1.75	0.46	B	CAMRW	4
HSC J1234+0007	188.6440	0.1190	1.04	...	2.13	1.78	0.63	B	CAM	...
HSC J1241+0347	190.4916	3.7893	0.34	0.414	3.37	1.63	0.52	B	R	...
HSC J1244+0413	191.2226	4.2208	0.33	0.322	4.66	2.75	0.46	A	RW	...
HSC J1249–0118	192.3172	–1.3085	0.48	...	9.11	1.56	0.83	B	W	...
HSC J1253+0437	193.4192	4.6181	0.22	0.243	4.60	3.00	0.00	A	W	...
HSC J1255+0102	193.8525	1.0358	0.34	0.374	10.38	1.63	0.52	B	RW	...
HSC J1308–0047	197.1898	–0.7886	0.18	0.188	11.22	2.33	0.47	B	W	...
HSC J1311–0120 <sup>K</sup>	197.8737	–1.3410	0.14	0.174	47.99	2.63	0.74	A	RW	17
HSC J1327+4305	201.8703	43.0833	0.36	0.374	10.78	2.75	0.46	A	RW	...
HSC J1337+0112 <sup>D</sup>	204.2834	1.2176	0.32	0.327	4.39	2.25	0.71	B	RW	4
HSC J1340+4410	205.1241	44.1676	0.44	0.546	5.96	2.33	0.47	B	...	...
HSC J1343+4155 <sup>K</sup>	205.8869	41.9175	0.40	0.418	12.83	3.00	0.00	A	RW	10
HSC J1349–0019†	207.2637	–0.3298	0.55	...	2.91	1.56	0.68	B	W	...
HSC J1400+0024	210.0880	0.4055	0.37	...	2.28	1.86	0.64	B	CAMRW	...
HSC J1407–0028	211.9735	–0.4715	0.49	0.471	10.32	2.29	0.70	B	CAMR	...
HSC J1410+0129 <sup>D</sup>	212.5043	1.4991	0.56	0.541	2.23	2.00	0.00	B	...	4, 6

**Table 3** – *continued*

Name	$\alpha$ (J2000)	$\delta$ (J2000)	$z_{\ell, \text{phot}}$	$z_{\ell, \text{spec}}$	$R_{\text{arc}}$ (arcsec)	Rank	$\sigma_{\text{Rank}}$	Grade	PC	References
HSC J1410–0109	212.7087	−1.1607	0.65	...	2.03	1.67	0.50	B	CAM	...
HSC J1411+0107 <sup>D</sup>	212.9073	1.1223	0.48	0.462	2.57	2.29	0.70	B	CAMW	4
HSC J1414–0136	213.5874	−1.6128	0.53	0.511	5.52	3.00	0.00	A	...	...
HSC J1418+0044	214.5233	0.7431	0.92	...	3.53	1.71	1.03	B	CAM	...
HSC J1419+0020†	214.7852	0.3469	0.36	0.339	4.25	2.29	0.70	B	...	...
HSC J1420+0057	215.0694	0.9547	0.49	0.507	10.96	2.29	0.70	B	RW	...
HSC J1420+0058 <sup>D</sup>	215.0743	0.9755	0.34	0.330	3.24	2.29	0.45	B	CAMW	4
HSC J1420+0007	215.2019	0.1258	0.58	0.545	3.67	2.29	0.70	B	CAM	...
HSC J1421+0022 <sup>D</sup>	215.2655	0.3720	0.67	...	2.29	2.29	0.45	B	CAM	2
HSC J1421–0024	215.4578	−0.4009	0.62	...	3.15	1.56	0.50	B	CAM	...
HSC J1423–0026†	215.9747	−0.4345	0.59	0.636	14.29	2.43	0.50	B	CAM	...
HSC J1424–0053 <sup>K</sup>	216.2042	−0.8892	0.87	0.795	3.33	2.86	0.35	A	CAM	4, 5, 11
HSC J1424+0042	216.2077	0.7004	0.47	0.477	5.29	1.57	0.50	B	CAMW	...
HSC J1427+0043 <sup>D</sup>	216.7776	0.7207	0.28	0.295	2.63	2.00	0.76	B	CAMW	4
HSC J1428+0043	217.0751	0.7252	0.32	0.335	8.48	1.57	0.50	B	CAMRW	...
HSC J1431–0006	217.8081	−0.1037	0.70	...	2.45	2.14	0.35	B	CAM	...
HSC J1434+4315	218.6586	43.2615	0.38	0.385	2.11	2.25	0.89	B	RW	...
HSC J1434–0056 <sup>D</sup>	218.7267	−0.9496	0.76	0.728	2.74	2.57	0.73	A	CAM	5
HSC J1435–0106	218.8296	−1.1101	0.78	...	2.69	1.78	0.67	B	CAM	...
HSC J1436+4329	219.0464	43.4891	0.39	0.386	2.70	3.00	0.00	A	W	...
HSC J1437–0002	219.3929	−0.0488	0.63	0.627	3.62	2.29	0.45	B	CAM	...
HSC J1441–0018	220.3623	−0.3164	0.35	0.287	5.32	2.29	0.45	B	...	...
HSC J1441–0053	220.3862	−0.8996	0.57	...	8.93	3.00	0.00	A	CAMW	...
HSC J1443+0102†	220.7898	1.0362	0.59	0.529	13.19	1.86	0.83	B	CAMW	...
HSC J1444–0051 <sup>D</sup>	221.1198	−0.8617	0.53	0.575	2.04	2.29	0.88	B	...	4, 5
HSC J1449–0002	222.4072	−0.0452	0.57	0.529	2.97	1.71	0.70	B	CAM	...
HSC J1450+0055	222.6666	0.9279	0.44	0.421	9.95	2.86	0.35	A	...	...
HSC J1451+0111 <sup>D</sup>	222.7769	1.1927	0.37	0.391	2.12	1.57	0.50	B	...	4
HSC J1458–0024 <sup>D</sup>	224.6513	−0.4000	0.65	0.595	3.93	2.29	0.45	B	CAMW	4
HSC J1459+4410	224.8790	44.1802	0.32	0.323	3.03	1.57	0.35	B	CAMRW	...
HSC J1459–0055	224.9882	−0.9230	0.60	0.939	2.22	1.56	0.68	B	CAMW	...
HSC J1507+4244	226.8466	42.7340	0.23	0.218	11.15	1.75	0.71	B	CAMRW	...
HSC J1508+4256	227.1544	42.9415	0.80	...	8.82	1.89	0.31	B	CAM	...
HSC J1510+4255	227.6903	42.9324	0.75	...	7.38	2.22	0.63	B	CAM	...
HSC J1513+4333	228.4882	43.5582	0.24	0.237	2.45	1.63	0.52	B	CAMRW	...
HSC J1522+4235	230.6975	42.5944	0.39	0.379	4.74	1.63	0.52	B	CAMRW	...
HSC J1525+4227	231.2877	42.4642	0.85	...	2.28	2.22	0.63	B	...	...
HSC J1525+4409	231.4855	44.1613	0.39	0.388	3.05	1.89	0.31	B	CAMR	...
HSC J1526+4406	231.6363	44.1044	0.48	0.487	2.15	1.67	0.47	B	...	...
HSC J1557+4206	239.3841	42.1066	0.46	...	2.15	2.33	0.67	B	...	...
HSC J1559+4232	239.8367	42.5423	0.85	...	4.37	1.56	0.50	B	CAM	...
HSC J1602+4346†	240.5990	43.7726	0.42	...	2.30	1.86	0.64	B	CAM	...
HSC J1602+4346	240.6045	43.7709	0.42	...	3.38	2.29	0.45	B	CAM	...
HSC J1602+4335	240.7110	43.5849	0.41	0.414	4.56	2.43	0.50	B	CAMRW	...
HSC J1602+4335	240.7214	43.5837	0.45	...	2.81	2.00	0.00	B	CAMRW	...
HSC J1618+4345	244.5774	43.7574	0.72	0.899	4.69	2.11	0.78	B	...	...
HSC J1618+5430	244.5857	54.5052	0.79	...	2.10	2.56	0.73	A	CAM	...
HSC J1620+4318	245.1101	43.3104	0.71	...	3.99	2.29	0.70	B	...	...
HSC J1621+4245	245.3623	42.7616	0.13	0.138	13.00	1.71	0.70	B	CAMRW	...
HSC J1629+4349	247.4261	43.8280	0.55	0.528	6.33	1.71	0.70	B	CAMRW	...
HSC J1631+4234†	247.7866	42.5781	0.68	...	2.12	1.57	0.90	B	CAM	...
HSC J1632+4246† <sup>D</sup>	248.2406	42.7699	0.22	0.228	2.20	3.00	0.00	A	W	16
HSC J2202+0234 <sup>D</sup>	330.7369	2.5761	0.49	0.482	6.60	2.29	0.70	B	CAMFRW	8
HSC J2203+0426	330.9438	4.4459	0.51	0.527	8.28	2.00	0.67	B	F	...
HSC J2205+0147 <sup>D</sup>	331.2789	1.7844	0.48	0.476	2.36	1.67	0.82	B	F	7
HSC J2205+0210†	331.3976	2.1760	0.26	0.252	3.29	1.56	0.68	B	W	...
HSC J2206+0411 <sup>D</sup>	331.6751	4.1919	0.53	0.537	4.24	1.56	0.68	B	FW	7
HSC J2207+0224†	331.8298	2.4046	0.42	0.418	3.50	2.29	0.70	B	CAMF	...
HSC J2208+0206	332.2499	2.1152	1.04	...	5.83	2.57	0.73	A	CAMF	...
HSC J2209–0034	332.4829	−0.5764	0.69	0.716	4.06	2.00	0.93	B	CAMF	...
HSC J2212–0008 <sup>D</sup>	333.0476	−0.1389	0.36	0.365	3.40	2.29	0.70	B	CAMFRW	1
HSC J2212+0650	333.1505	6.8415	0.38	0.399	2.04	2.00	0.00	B	RW	...
HSC J2213–0018 <sup>D</sup>	333.2770	−0.3084	0.40	0.408	7.60	1.57	0.50	B	CAMFRW	1
HSC J2213–0030 <sup>K</sup>	333.2789	−0.5103	0.64	0.702	2.75	1.57	0.90	B	CAMF	7, 18

**Table 3** – *continued*

Name	$\alpha$ (J2000)	$\delta$ (J2000)	$z_{\ell, \text{phot}}$	$z_{\ell, \text{spec}}$	$R_{\text{arc}}$ (arcsec)	Rank	$\sigma_{\text{Rank}}$	Grade	PC	References
HSC J2213+0354†	333.3342	3.9100	0.69	0.670	5.01	2.44	0.50	B	CAM	...
HSC J2213+0048 <sup>XK</sup>	333.3826	0.8100	0.95	...	5.19	2.29	0.45	B	F	7, 18
HSC J2213+0056	333.4550	0.9475	0.28	...	3.14	1.57	0.50	B	CAM	...
HSC J2214+0110 <sup>D</sup>	333.5787	1.1772	0.63	0.566	3.57	1.57	0.90	B	CAMFW	1, 7
HSC J2215+0102 <sup>D</sup>	333.8056	1.0446	0.71	...	2.26	1.89	0.60	B	CAMF	1
HSC J2215+0435	333.9658	4.5838	0.65	...	9.39	2.22	0.63	B	CAMW	...
HSC J2217-0038	334.3723	-0.6436	0.30	...	2.06	1.56	0.50	B	...	...
HSC J2221-0053 <sup>K</sup>	335.4324	-0.8842	0.34	0.334	4.98	1.78	0.42	B	CAM	18
HSC J2226+0041 <sup>X C</sup>	336.5386	0.6949	0.63	0.647	2.98	3.00	0.00	A	...	1, 3, 5
HSC J2226-0034	336.6597	-0.5805	0.38	0.404	2.20	1.78	0.42	B	CAMR	...
HSC J2228+0022	337.1687	0.3704	0.59	...	1.21	2.00	0.54	B	...	...
HSC J2230-0018†	337.5731	-0.3125	0.40	0.406	7.05	1.57	1.05	B	CAMR	...
HSC J2232+0057	338.0466	0.9501	0.40	0.401	2.38	1.71	0.45	B	CAMW	...
HSC J2232-0025	338.1611	-0.4261	1.08	...	2.13	3.00	0.00	A	CAM	...
HSC J2233-0104 <sup>X</sup>	338.3201	-1.0694	0.95	...	22.15	1.57	1.05	B	...	...
HSC J2233-0019	338.3331	-0.3264	0.45	0.398	4.13	1.57	0.73	B	CAMR	...
HSC J2233+0157	338.4742	1.9560	0.27	...	2.08	2.22	0.63	B	CAMR	...
HSC J2235-0135	338.8841	-1.5944	0.48	...	3.05	1.56	0.96	B	W	...
HSC J2235+0003	338.9535	0.0509	0.76	0.735	8.66	1.71	0.70	B	CAM	...
HSC J2236+0616	339.0586	6.2723	0.37	0.350	3.40	2.13	0.64	B	W	...
HSC J2239+0235	339.8946	2.5853	1.13	...	1.91	3.00	0.00	A	CAM	...
HSC J2242+0011 <sup>D</sup>	340.5899	0.1956	0.39	0.385	2.43	3.00	0.00	A	CAMR	5
HSC J2243-0004	340.9990	-0.0803	0.71	0.690	3.31	1.71	0.00	B	...	...
HSC J2246+0558†	341.5610	5.9748	0.31	0.340	2.66	2.63	0.74	A	RW	...
HSC J2246+0415	341.6871	4.2637	1.02	...	8.67	2.33	0.47	B	CAM	...
HSC J2248+0147 <sup>D</sup>	342.2457	1.7865	0.38	0.360	6.74	2.00	0.00	B	CAMRW	5
HSC J2258+0031	344.5655	0.5248	0.26	0.256	4.80	1.75	0.46	B	CAMRW	...
HSC J2306+0225 <sup>D</sup>	346.7428	2.4286	0.35	0.362	3.17	2.00	0.00	B	CAMRW	6
HSC J2313-0104 <sup>C</sup>	348.4770	-1.0802	0.53	0.531	8.13	2.63	0.52	A	...	1, 15
HSC J2314-0003	348.5673	-0.0529	0.60	...	2.64	1.56	0.68	B	W	...
HSC J2315+0129 <sup>D</sup>	348.9799	1.4850	0.46	0.424	3.68	1.56	0.83	B	CAMRW	6
HSC J2319+0038	349.9726	0.6369	0.94	...	7.69	2.33	0.82	B	CAM	...
HSC J2328+0005	352.2238	0.0937	0.50	0.443	3.67	2.00	0.00	B	CAM	...
HSC J2329-0120 <sup>C</sup>	352.4494	-1.3466	0.53	0.537	10.50	1.67	0.94	B	CAMW	1, 15
HSC J2330+0133	352.5252	1.5512	0.42	0.444	3.44	1.67	0.67	B	CAMW	...
HSC J2330+0158	352.6815	1.9702	0.69	...	2.16	1.67	0.82	B	CAM	...
HSC J2332-0003	353.1491	-0.0511	0.52	0.510	3.76	1.71	0.45	B	CAMR	...
HSC J2337+0016	354.4175	0.2781	0.32	0.272	2.00	3.00	0.00	A	R	...
HSC J2346-0010	356.5148	-0.1829	0.26	0.261	2.30	1.56	0.68	B	RW	...
HSC J2351+0037	357.8388	0.6169	0.26	0.277	2.96	2.63	0.52	A	CAMRW	...
HSC J2352+0006	358.0488	0.1041	0.67	...	1.61	1.56	0.68	B	...	...
HSC J2359+0208 <sup>D</sup>	359.8898	2.1399	0.44	0.430	8.67	2.88	0.35	A	CAMRW	2

Note. References: <sup>1</sup>Diehl et al. (2017), <sup>2</sup>Huang et al. (2019), <sup>3</sup>Jacobs et al. (2019), <sup>4</sup>Petrillo et al. (2019), <sup>5</sup>Sonnenfeld et al. (2018), <sup>6</sup>Wong et al. (2018), <sup>7</sup>More et al. (2012), <sup>8</sup>More et al. (2016), <sup>9</sup>Cabanac et al. (2007), <sup>10</sup>Stark et al. (2013), <sup>11</sup>Tanaka et al. (2016), <sup>12</sup>Bolton et al. (2008), <sup>13</sup>Faure et al. (2008), <sup>14</sup>Hammer (1991), <sup>15</sup>Carrasco et al. (2017), <sup>16</sup>Chan et al. (2020), <sup>17</sup>Tyson, Valdes & Wenk (1990), <sup>18</sup>Limousin et al. (2009), <sup>19</sup>Auger et al. (2013).

frames. The resulting rectified orders are then shifted, co-added, and flux calibrated to obtain the final two-dimensional (2D) spectrum. For further data processing and analysis, we use standard IRAF tools. We produce one-dimensional (1D) spectra using an extraction aperture in all three arms and for all three images of the source (apertures are shown by red and blue dashed line on Fig. 6).

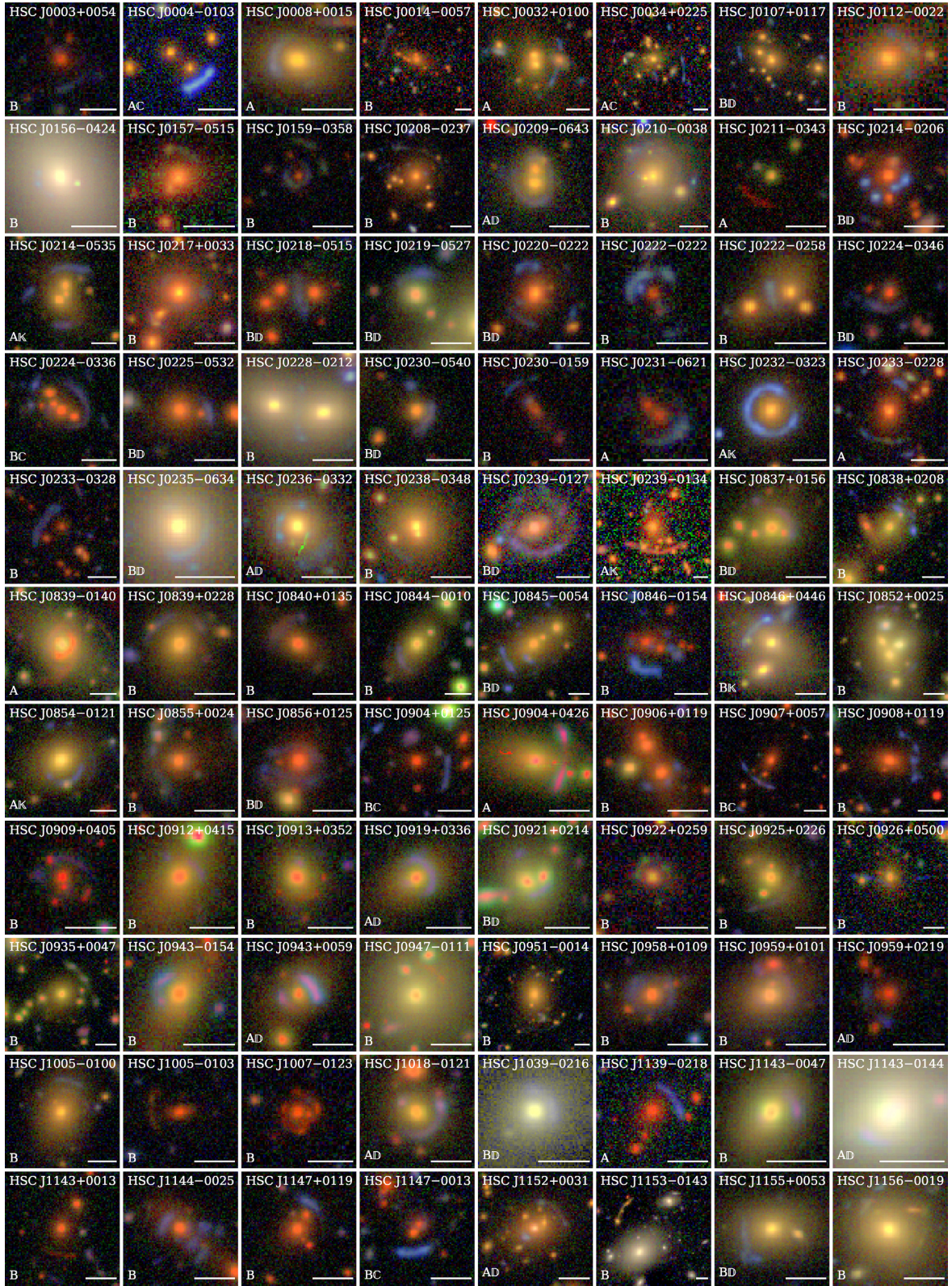
### 5.1 Redshift measurement

We visually inspected all of the three arms of the X-shooter (2D and 1D) spectra in order to identify any emission and/or absorption lines arising from the lensed galaxies. We identified a set of emission lines that could be attributed to a common redshift. We fitted Gaussian profiles to each of those lines in order to determine their central wavelength and, thereby, determined a mean redshift for each lensed galaxy. Most of the lensed arcs showed [O II]

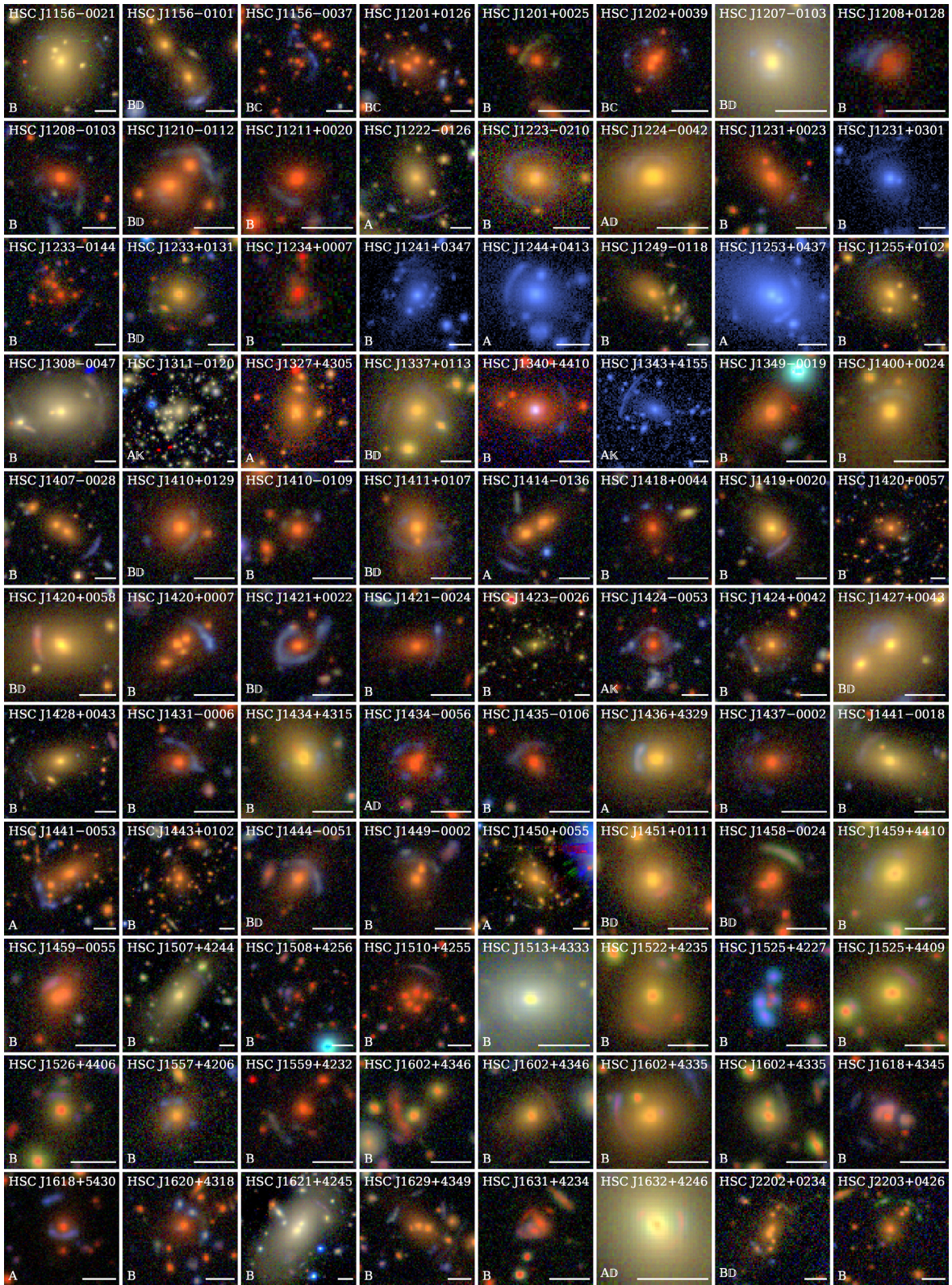
doublet  $\lambda 3726.03, 3728.81$  Å, H  $\delta$   $\lambda 4101.73$  Å, H  $\gamma$   $\lambda 4340.46$  Å, H  $\beta$   $\lambda 4861.32$  Å, [O III]  $\lambda 4958.91, 5006.84$  Å, H  $\alpha$   $\lambda 6562.79$  Å, [N II]  $\lambda 6583.45$  Å, [S II]  $\lambda 6716.43$ , and  $\lambda 6730.81$  Å, which are expected to be found in blue star-forming galaxies. Our lensed galaxies span a redshift range from  $z \sim 0.9$  to 2.2 (summarized in Table 4). We give a short description of the confirmed lenses below.

### 5.2 Spectroscopically confirmed group-scale lenses

*HSC J0224-0336* at  $z_{\ell, \text{spec}} = 0.613$ : This system has been reported in More et al. (2012) and has four bright early-type galaxies at the centre, surrounded by a blue arc (almost complete ring). We set the slit along the arc to the north-west of the lens (see Fig. 6) that has a peak flux in  $g$  band. Most of the emission lines in this



**Figure 4.** SuGOHI-c lens candidates with grades A and B (shown on the bottom left). Spectroscopically confirmed, previously discovered, or known lenses are indicated by 'C', 'D', or 'K', respectively. All images are oriented with North up and East left. Scale bars of 5 arcsec are displayed in the bottom right corner.

**Figure 4.** – *Continued.*

system are detected in the NIR arm of X-shooter, H  $\beta$ , [O III], H  $\alpha$ , [N II], and [S II]. We also detected the [O II] doublet in the VIS arm. These emission lines correspond to a mean redshift of  $z = 1.514$ . The lens galaxy, 'G' of HSC J0224–0336 shown in Fig. 6,

is identified as the centre of the cluster by Wen et al. (2012), which has a richness of  $N_{\text{ric}, \text{WEN}} = 21.62$  with 14 member galaxies and corresponds to  $M_{200} \approx 1.18 \times 10^{14} M_\odot$ . However, the same galaxy is identified as a member galaxy of a cluster, in CAMIRA, with a

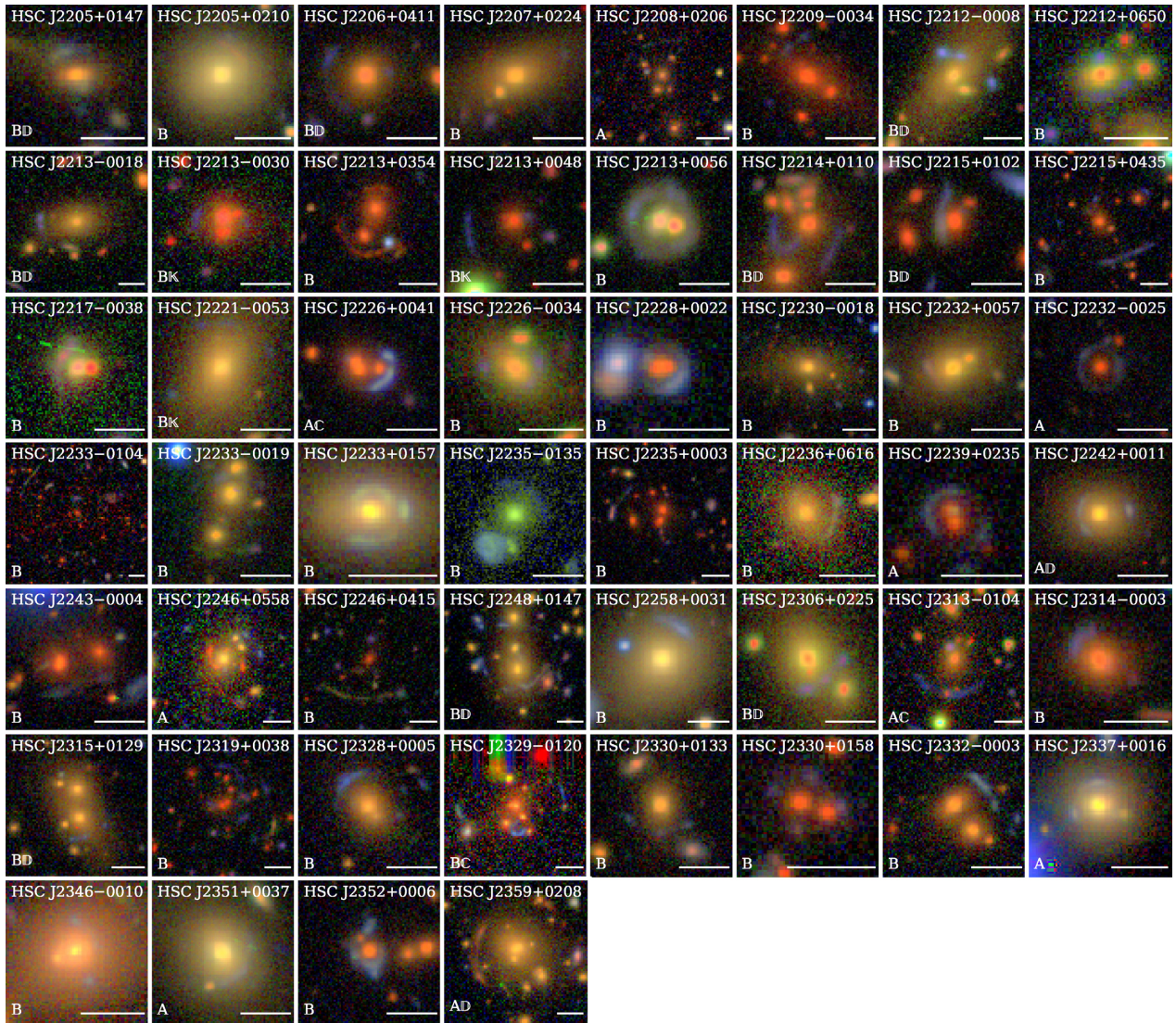


Figure 4. – Continued.

richness of  $N_{\text{ric,CAMIRA}} = 19.62$ , 63 member galaxies, and  $M_{200} \approx 6.36 \times 10^{13} M_{\odot}$ . The stellar velocity dispersion of the lens galaxy is  $448 \pm 101 \text{ km s}^{-1}$  from the SDSS data.

*HSCJ0904+0125* at  $z_{\ell,\text{phot}} = 0.914$ : For this system, we set the slit along a nearly north–south blue arc. We detected emission lines such as the [O II] doublet, H $\beta$ , [O III], and H $\alpha$  in NIR arm corresponding to a mean redshift of  $z = 2.176$ . The lens galaxy of the system, 'G' in HSCJ0904+0125 panel of Fig. 6, is identified as the galaxy member in CAMIRA. The cluster has a richness  $N_{\text{ric,CAMIRA}} = 18.37$  with 56 member galaxies and corresponds to  $M_{200} \approx 5.83 \times 10^{13} M_{\odot}$ .

*HSC J0907+0057* at  $z_{\ell,\text{phot}} = 0.723$ : This system is composed of a number of blue arcs around a bright early-type galaxy at a separation  $\simeq 5$  arcsec. We set a slit along the east-most arc-like component whose light is not contaminated by any red blobs (see Fig. 4). We detect weak emission lines such as the [O II] doublet and [O III] $\lambda 5008.24 \text{ \AA}$  line, yielding a lensed galaxy redshift of  $z = 1.916$ . The lens galaxy, 'G' of HSC J0907+0057 shown in Fig. 6, is at the centre of the cluster in CAMIRA, which has a richness of  $N_{\text{ric,CAMIRA}} = 35.49$  and 75 member galaxies corresponding to  $M_{200} \approx 1.38 \times 10^{14} M_{\odot}$ .

*HSC J1147-0013* at  $z_{\ell,\text{phot}} = 0.805$ : We detect many strong emission lines such as [O II] doublet, H $\gamma$ , H $\beta$ , [O III], and H $\alpha$  in the NIR arm from the nearly straight blue arcs. This system has similar features to HSC J0904+0125, which has a small peak near main peak. We find that the emission lines correspond to a mean redshift of  $z = 2.093$ . This group-scale system is found serendipitously during the inspection owing to the very bright arc next to another cluster. The cluster catalogues may have missed this due to lack of sufficiently bright galaxies.

*HSC J1156-0037* at  $z_{\ell,\text{phot}} = 0.918$ : We find that the blue arc has a mean redshift of  $z = 1.907$  from the emission lines [O II] doublet, H $\gamma$ , H $\beta$ , [O III], and H $\alpha$  in the NIR arm. The lens galaxy, 'G' of HSC J1156-0037 shown in Fig. 6, is found to be a galaxy member of the large cluster in CAMIRA, which has a high richness of  $N_{\text{ric,CAMIRA}} = 64.05$  corresponding to  $M_{200} \approx 3.00 \times 10^{14} M_{\odot}$ . This cluster has 126 member galaxies.

*HSC J1201+0126* at  $z_{\ell,\text{phot}} = 0.618$ : This system has been reported in Petrillo et al. (2019). We set the slit along the blue arc, which has a small early-type galaxy included (which produces the continuum in the 2D spectra). We detect weak continuum from early-type galaxy and strong emission lines, H $\beta$ , [O III] and H $\alpha$  in

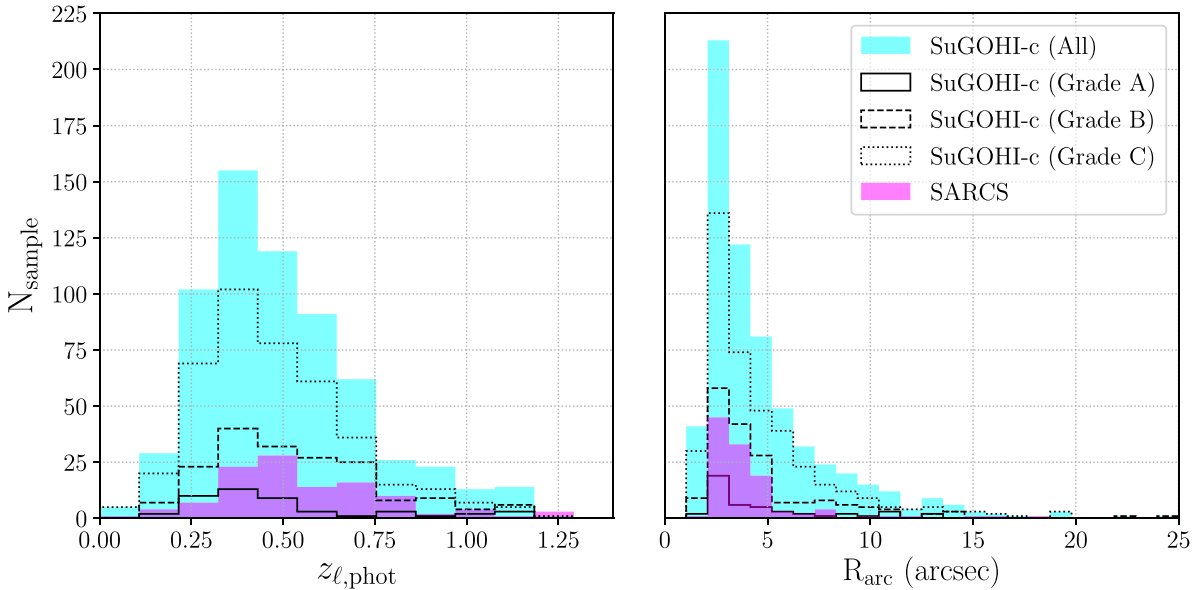


**Figure 5.** *Left:* Photometric redshift distributions of group-to-cluster-scale lens candidates. The peak of the redshift distributions for both the SuGOHI-c sample (cyan) and the SARCS sample (magenta, More et al. 2012) is around  $z \sim 0.4$ . *Right:* The binned distribution of arc radii for  $R_{\text{arc}} \geq 2$ . The peak at around 3 arcsec attests to the fact that most of the candidates are, indeed, at group scales. As before, cyan and magenta show the SuGOHI-c and the SARCS samples, respectively.

NIR arm and [O II] doublet in VIS arm, yielding a lensed galaxy redshift of  $z = 1.653$ . The lens galaxy, 'G' of HSC J1201+0126 shown in Fig. 6, is at the centre of the cluster as per CAMIRA, which has a richness of  $N_{\text{ric,CAMIRA}} = 36.23$  with 67 member galaxies and corresponds to  $M_{200} \approx 1.42 \times 10^{14} M_{\odot}$ .

*HSC J1202+0039* at  $z_{\ell,\text{spec}} = 0.689$ : As seen in Fig. 6, the slit targeting this system covers the source in two locations, the East and North of the lens. We detect strong emission lines [O III]  $\lambda 4960.30 \text{ \AA}$  and [O III]  $\lambda 5008.24 \text{ \AA}$  in each source location. We find that the emission lines have a mean redshift of  $z = 1.885$ . The lens galaxy, 'G' of HSC J1202+0039 shown in Fig. 6, is identified as the BCG as per CAMIRA, which has a richness of  $N_{\text{ric,CAMIRA}} = 36.298$  with 75 member galaxies and corresponding to  $M_{200} \approx 1.42 \times 10^{14} M_{\odot}$ . The stellar velocity dispersion of the BCG is  $238 \pm 37 \text{ km s}^{-1}$  from the SDSS data.

*HSC J2213+0048* at  $z_{\ell,\text{phot}} = 0.945$ : We do not detect continuum or any features from emission or absorption in the spectrum of this system. The lens galaxy, 'G' of HSC J2213+0048 shown in Fig. 6, is identified as a member of a group in Ford et al. (2015), which has a richness of  $N_{\text{ric,FORD}} = 8.80$  with 68 member galaxies, corresponding to  $M_{200} \approx 7.29 \times 10^{12} M_{\odot}$ . This system also has been reported in More et al. (2012). *HSC J2226+0041* at  $z_{\ell,\text{spec}} = 0.647$ : This is a known lens system (Diehl et al. 2017; Sonnenfeld et al. 2018; Jacobs et al. 2019). We measure a mean redshift of  $z = 1.897$  from emission lines such as [O II] (assuming the rest-frame centroid of the unresolved [O II] doublet  $\lambda 3728.3 \text{ \AA}$ ), H  $\gamma$ , H  $\beta$ , [O III]  $\lambda 4960.30 \text{ \AA}$ , [O III]  $\lambda 5008.24 \text{ \AA}$ , and H  $\alpha$ . The stellar velocity dispersion of the lens galaxy, 'G' of HSC J2226+0041 shown in Fig. 6, is  $318 \pm 47 \text{ km s}^{-1}$  from the SDSS data.

*HSC J2233–0104* at  $z_{\ell,\text{phot}} = 0.953$ : We detect three probable blue arcs: a long-thin arc and a short arc to the north-east of the lens, and a third short arc to the north of the lens (see Fig. 7). We set the slit along the northern arc and detect some emission lines: an unresolved [O II] doublet  $\lambda 3728.30$ , [O III]  $\lambda 4960.30 \text{ \AA}$ , [O III]  $\lambda 5008.24 \text{ \AA}$ , H  $\alpha$ , [N II], and also weak emission of H  $\beta$ . The

emission lines suggest a mean redshift of  $z = 0.902$ , indicating that the arc is probably not a lensed galaxy since the redshift of this arc is close to the photometric redshift of the lens galaxy, 'G' of HSC J2233–0104 shown in Fig. 6.

## 6 SUMMARY AND CONCLUSION

We have carried out the largest ever systematic search for strong gravitational lens systems at group-to-cluster-scales. Since the S18A release of the HSC–SSP Survey, covering nearly  $1114 \text{ deg}^2$ , we have visually inspected 39 435 groups and clusters selected from four parent cluster catalogues. While CAMIRA catalogue was obtained from HSC imaging, other catalogues (Wen et al. 2012; Ford et al. 2015; Rykoff et al. 2016) came from previous surveys with overlapping footprints.

Our search resulted in a total of 641 lens candidates with 228 highly promising (grade A-B) candidates and 413 plausible (grade C) candidates. Additionally, we report 131 galaxy-scale lens candidates found serendipitously during our search. Most of these are new and are missed from the previously reported SuGOHI-g samples (see Appendix A).

The SuGOHI-c will enable detailed studies of mass distributions in individual systems for even low-mass galaxy groups at low-to-intermediate redshifts and clusters at very high redshifts. Furthermore, the large sample size will surpass any of the previous statistical studies of group-scale lenses. Finally, we have nearly six times more lenses at high redshifts ( $z_{\ell} > 0.8$ ) compared to the previous high-redshift SARCS sample. Thus, we will be able to study evolution in the mass distributions at these mass scales for the first time.

The SuGOHI-c sample has many striking systems with blue giant arcs, red-lensed galaxies, and in some cases, multiple-lensed galaxies from distinct redshifts lensed by the same galaxy groups. We also present the results of our spectroscopic follow-up with X-shooter where, for nine out of the 10 candidates, we could detect

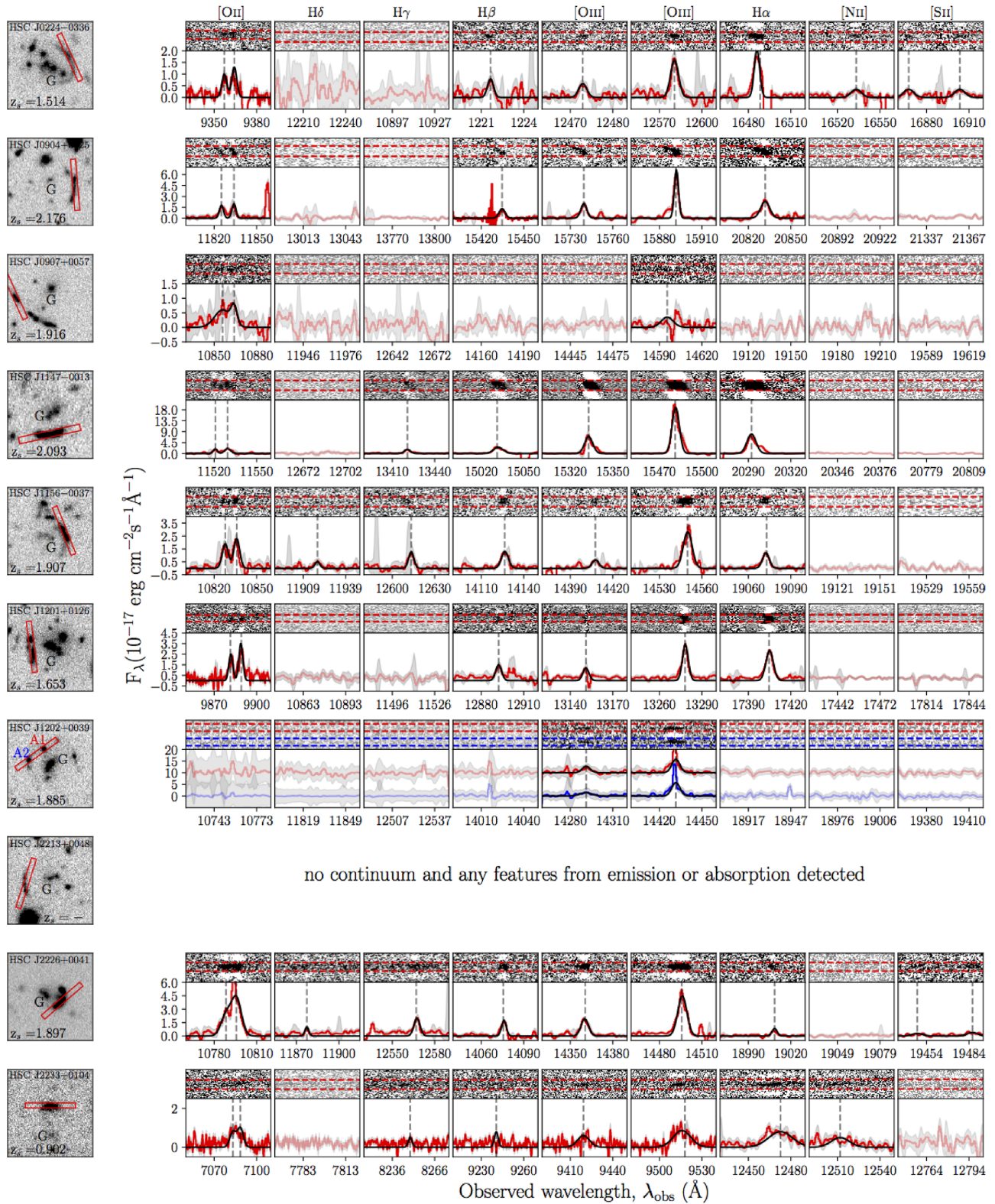


**Figure 6.** Spectroscopic results from the X-shooter observations. Each row is for one candidate lens. One candidate (HSC J2213+0048) with no detection is shown in image only here. On the left, we show the alignment of the slit on the putative lensed source that was observed. The brightest lens galaxies are denoted by 'G'. On the right, the upper panel (for each row) shows regions from the 2D spectrum where interesting features are expected. The red (and blue) dashed lines show the exact region used for extracting the 1D spectrum of one of the lensed images (and its counterpart). The bottom panel shows the corresponding stacked 1D spectra (red) where the vertical lines highlight the location of expected emission lines. The labels for those emission lines are shown at the top of the figure. The error on the spectrum is shown by a shaded region (grey) and Gaussian fits to the emission lines are in black. The semi-transparent panels show the locations of some of the common emission lines, which are not detected, for the given source redshift.

**Table 4.** Summary of X-shooter spectroscopic observations. Position angles (PA) are measured east of north.

Name	Obs. Date (UT)	PA (deg)	$z_s$
HSC J0224–0336	13-07-2017	25	1.514
HSC J0904+0125	09-04-2017	5	2.176
HSC J0907+0057	29-01-2018	25	1.916
HSC J1147–0013	28-02-2018	102	2.093
HSC J1156–0037	07-04-2017	22	1.907
HSC J1201+0126	07-04-2017	7	1.653
HSC J1202+0039	06-04-2017 01-03-2018	–55	1.885
HSC J2213+0048	10-06-2017 15-08-2017	–18	–
HSC J2226+0041	29-09-2017	–50	1.897
HSC J2233–0104	07-08-2017	90	0.902

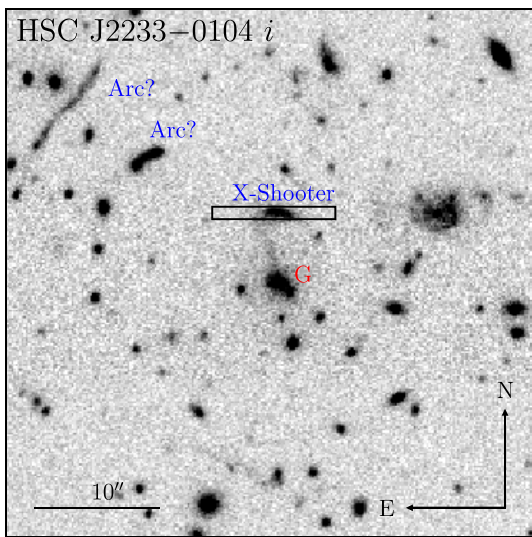


**Figure 7.** HSC J2233–0104 lens candidate. Image is  $\sim 43$  arcsec on the side. The bar shows a scale of 10 arcsec.

emission lines and successfully measure the redshifts of the lensed galaxies. A detailed mass modelling analysis using spectroscopic results will be presented in the near future.

## ACKNOWLEDGEMENTS

The authors would like to thank the referee for improving the presentation of the paper. ATJ and KTI are supported by JSPS KAKENHI Grant Number JP17H02868. MO is supported by JSPS KAKENHI Grant Number JP15H05892 and JP18K03693. IK is supported by JSPS KAKENHI Grant Number JP15H05896. SHS thanks the Max Planck Society for support through the Max Planck Research Group. JHHC acknowledges support from the Swiss National Science Foundation (SNSF). This work was supported in part by World Premier International Research centre Initiative (WPI Initiative), MEXT, Japan.

The Hyper Suprime-Cam (HSC) collaboration includes the astronomical communities of Japan and Taiwan, and Princeton University. The HSC instrumentation and software were developed by the National Astronomical Observatory of Japan (NAOJ), the Kavli Institute for the Physics and Mathematics of the Universe (Kavli IPMU), the University of Tokyo, the High Energy Accelerator

Research Organization (KEK), the Academia Sinica Institute for Astronomy and Astrophysics in Taiwan (ASIAA), and Princeton University. Funding was contributed by the FIRST program from the Japanese Cabinet Office, the Ministry of Education, Culture, Sports, Science and Technology (MEXT), the Japan Society for the Promotion of Science (JSPS), Japan Science and Technology Agency (JST), the Toray Science Foundation, NAOJ, Kavli IPMU, KEK, ASIAA, and Princeton University.

This paper makes use of software developed for the Large Synoptic Survey Telescope. We thank the LSST Project for making their code available as free software at <http://dm.lsst.org>.

This paper is based [in part] on data collected at the Subaru Telescope and retrieved from the HSC data archive system, which is operated by Subaru Telescope and Astronomy Data Center (ADC) at NAOJ. Data analysis was in part carried out with the cooperation of Center for Computational Astrophysics (CfCA), NAOJ.

The Pan-STARRS1 Surveys (PS1) and the PS1 public science archive have been made possible through contributions by the Institute for Astronomy, the University of Hawaii, the Pan-STARRS Project Office, the Max-Planck Society and its participating institutes, the Max Planck Institute for Astronomy, Heidelberg, and the Max Planck Institute for Extraterrestrial Physics, Garching, The Johns Hopkins University, Durham University, the University of Edinburgh, Queen's University Belfast, the Harvard-Smithsonian centre for Astrophysics, the Las Cumbres Observatory Global Telescope Network Incorporated, the National Central University of Taiwan, the Space Telescope Science Institute, the National Aeronautics and Space Administration under Grant No. NNX08AR22G issued through the Planetary Science Division of the NASA Science Mission Directorate, the National Science Foundation under Grant No. AST-1238877, the University of Maryland, Eotvos Lorand University (ELTE), the Los Alamos National Laboratory, and the Gordon and Betty Moore Foundation.

Based (in part) on data collected at the Subaru Telescope and retrieved from the HSC data archive system, which is operated by Subaru Telescope and Astronomy Data centre at National Astronomical Observatory of Japan.

Funding for the SDSS IV has been provided by the Alfred P. Sloan Foundation, the U.S. Department of Energy Office of Science, and the Participating Institutions. SDSS acknowledges support and resources from the centre for High-Performance Computing at the University of Utah. The SDSS website is [www.sdss.org](http://www.sdss.org).

SDSS is managed by the Astrophysical Research Consortium for the Participating Institutions of the SDSS Collaboration including the Brazilian Participation Group, the Carnegie Institution for Science, Carnegie Mellon University, the Chilean Participation Group, the French Participation Group, Harvard-Smithsonian centre for Astrophysics, Instituto de Astrofísica de Canarias, the Johns Hopkins University, Kavli Institute for the Physics and Mathematics of the Universe (IPMU)/University of Tokyo, the Korean Participation Group, Lawrence Berkeley National Laboratory, Leibniz Institut für Astrophysik Potsdam (AIP), Max-Planck-Institut für Astronomie (MPIA Heidelberg), Max-Planck-Institut für Astrophysik (MPA Garching), Max-Planck-Institut für Extraterrestrische Physik (MPE), National Astronomical Observatories of China, New Mexico State University, New York University, University of Notre Dame, Observatório Nacional/MCTI, The Ohio State University, Pennsylvania State University, Shanghai Astronomical Observatory, United Kingdom Participation Group, Universidad Nacional Autónoma de México, University of Arizona, University of Colorado Boulder, University of Oxford, University of Portsmouth, University of Utah, University of Virginia, University

of Washington, University of Wisconsin, Vanderbilt University, and Yale University.

## REFERENCES

- Aguado D. S. et al., 2019, *ApJS*, 240, 23  
 Aihara H. et al., 2018a, *PASJ*, 70, S4  
 Aihara H. et al., 2018b, *PASJ*, 70, S8  
 Aihara H. et al., 2019, *PASJ*, 71, 114  
 Auger M. W., Budzynski J. M., Belokurov V., Koposov S. E., McCarthy I. G., 2013, *MNRAS*, 436, 503  
 Axelrod T., Kantor J., Lupton R. H., Pierfederici F., 2010, Proc. SPIE Conf. Ser., Software and Cyberinfrastructure for Astronomy, Vol. 7740. SPIE, Bellingham, p. 774015  
 Balogh M. L. et al., 2009, *MNRAS*, 398, 754  
 Balogh M. L. et al., 2011, *MNRAS*, 412, 2303  
 Barnabè M., Czoske O., Koopmans L. V. E., Treu T., Bolton A. S., Gavazzi R., 2009, *MNRAS*, 399, 21  
 Bartelmann M., Huss A., Colberg J. M., Jenkins A., Pearce F. R., 1998, *A&A*, 330, 1  
 Bolton A. S., Burles S., Koopmans L. V. E., Treu T., Gavazzi R., Moustakas L. A., Wayth R., Schlegel D. J., 2008, *ApJ*, 682, 964  
 Bonvin V. et al., 2017, *MNRAS*, 465, 4914  
 Bosch J. et al., 2018, *PASJ*, 70, S5  
 Cabanac R. A. et al., 2007, *A&A*, 461, 813  
 Carrasco M. et al., 2017, *ApJ*, 834, 210  
 Chan J. H. H. et al., 2020, *A&A*, 636, A87  
 Coupon J., Czakon N., Bosch J., Komiya Y., Medezinski E., Miyazaki S., Oguri M., 2018, *PASJ*, 70, S7  
 Dai X., Bregman J. N., Kochanek C. S., Rasia E., 2010, *ApJ*, 719, 119  
 Dark Energy Survey Collaboration, 2016, *MNRAS*, 460, 1270  
 de Jong J. T. A. et al., 2015, *A&A*, 582, A62  
 Dey A. et al., 2019, *AJ*, 157, 168  
 Diehl H. T. et al., 2017, *ApJS*, 232, 15  
 Eisenstein D. J. et al., 2011, *AJ*, 142, 72  
 Faure C. et al., 2008, *ApJS*, 176, 19  
 Faure C. et al., 2011, *A&A*, 529, A72  
 Ferreras I., Saha P., Leier D., Courbin F., Falco E. E., 2010, *MNRAS*, 409, L30  
 Ford J., Hildebrandt H., Van Waerbeke L., Erben T., Laigle C., Milkereit M., Morrison C. B., 2014, *MNRAS*, 439, 3755  
 Ford J. et al., 2015, *MNRAS*, 447, 1304  
 Foëx G., Motta V., Jullo E., Limousin M., Verdugo T., 2014, *A&A*, 572, A19  
 Foëx G., Motta V., Limousin M., Verdugo T., More A., Cabanac R., Gavazzi R., Muñoz R. P., 2013, *A&A*, 559, A105  
 Freudling W., Romaniello M., Bramich D. M., Ballester P., Forchi V., García-Dabló C. E., Moehler S., Neeser M. J., 2013, *A&A*, 559, A96  
 Furusawa H. et al., 2018, *PASJ*, 70, S3  
 Gavazzi R., Treu T., Rhodes J. D., Koopmans L. V. E., Bolton A. S., Burles S., Massey R. J., Moustakas L. A., 2007, *ApJ*, 667, 176  
 Gladders M. D., Hoekstra H., Yee H. K. C., Hall P. B., Barrientos L. F., 2003, *ApJ*, 593, 48  
 Grillo C., 2010, *ApJ*, 722, 779  
 Hammer F., 1991, *ApJ*, 383, 66  
 Helsdon S. F., Ponman T. J., 2000, *MNRAS*, 315, 356  
 Heymans C. et al., 2012, *MNRAS*, 427, 146  
 Hezaveh Y. D. et al., 2016, *ApJ*, 823, 37  
 Hsieh B. C., Yee H. K. C., 2014, *ApJ*, 792, 102  
 Huang S. et al., 2018, *PASJ*, 70, S6  
 Huang X. et al., 2019, preprint ([arXiv:1906.00970](https://arxiv.org/abs/1906.00970))  
 Ivezić Ž. et al., 2008, *Serb. Astron. J.*, 176, 1  
 Ivezić Ž. et al., 2019, *ApJ*, 873, 111  
 Jacobs C. et al., 2019, *ApJS*, 243, 17  
 Jaelani A. T. et al., 2020, *MNRAS*, 494, 3156  
 Jurić M. et al., 2017, in Lorente N. P. F., Shortridge K., Wayth R., eds, ASP Conf. Ser., Vol. 512, Astronomical Data Analysis Software and Systems XXV. Astron. Soc. Pac., San Francisco, p. 279  
 Kawanomoto S. et al., 2018, *PASJ*, 70, 66  
 Komiya Y. et al., 2018, *PASJ*, 70, S2  
 Koopmans L. V. E., Treu T., 2003, *ApJ*, 583, 606  
 Koopmans L. V. E., Treu T., Bolton A. S., Burles S., Moustakas L. A., 2006, *ApJ*, 649, 599  
 Koopmans L. V. E. et al., 2009, in astro2010: The Astronomy and Astrophysics Decadal Survey. p. 159, preprint ([arXiv:0902.3186](https://arxiv.org/abs/0902.3186))  
 Krusch E., Rosenbaum D., Dettmar R. J., Bomans D. J., Taylor C. L., Aronica G., Elwert T., 2006, *A&A*, 459, 759  
 Limousin M. et al., 2009, *A&A*, 502, 445  
 Mandelbaum R., Seljak U., Hirata C. M., 2008, *J. Cosmology Astropart. Phys.*, 8, 006  
 Marshall P. J. et al., 2016, *MNRAS*, 455, 1171  
 Milkereit M., van Waerbeke L., Heymans C., Hildebrandt H., Dietrich J. P., Erben T., 2010, *MNRAS*, 406, 673  
 Miyazaki S. et al., 2018, *PASJ*, 70, S1  
 Modigliani A. et al., 2010, Proc. SPIE, 7737, 773728  
 More A., Cabanac R., More S., Alard C., Limousin M., Kneib J. P., Gavazzi R., Motta V., 2012, *ApJ*, 749, 38  
 More A., Jahnke K., More S., Gallazzi A., Bell E. F., Barden M., Häubler B., 2011, *ApJ*, 734, 69  
 More A., McKean J. P., More S., Porcas R. W., Koopmans L. V. E., Garrett M. A., 2009, *MNRAS*, 394, 174  
 More A., McKean J. P., Muxlow T. W. B., Porcas R. W., Fassnacht C. D., Koopmans L. V. E., 2008, *MNRAS*, 384, 1701  
 More A. et al., 2016, *MNRAS*, 455, 1191  
 Murata R. et al., 2019, *PASJ*, 71, 107  
 Newman A. B., Ellis R. S., Treu T., 2015, *ApJ*, 814, 26  
 Oguri M., 2006, *MNRAS*, 367, 1241  
 Oguri M., 2014, *MNRAS*, 444, 147  
 Oguri M., Bayliss M. B., Dahle H., Sharon K., Gladders M. D., Natarajan P., Hennawi J. F., Koester B. P., 2012, *MNRAS*, 420, 3213  
 Oguri M. et al., 2018, *PASJ*, 70, S20  
 Parker L. C., Hudson M. J., Carlberg R. G., Hoekstra H., 2005, *ApJ*, 634, 806  
 Petrillo C. E. et al., 2019, *MNRAS*, 484, 3879  
 Richard J., Jones T., Ellis R., Stark D. P., Livermore R., Swinbank M., 2011, *MNRAS*, 413, 643  
 Rines K., Diaferio A., 2010, *AJ*, 139, 580  
 Ruff A. J., Gavazzi R., Marshall P. J., Treu T., Auger M. W., Brault F., 2011, *ApJ*, 727, 96  
 Rykoff E. S. et al., 2014, *ApJ*, 785, 104  
 Rykoff E. S. et al., 2016, *ApJS*, 224, 1  
 Sonnenfeld A. et al., 2020, preprint ([arXiv:2002.01611](https://arxiv.org/abs/2002.01611))  
 Sonnenfeld A., Jaelani A. T., Chan J., More A., Suyu S. H., Wong K. C., Oguri M., Lee C.-H., 2019, *A&A*, 630, A71  
 Sonnenfeld A., Treu T., Gavazzi R., Marshall P. J., Auger M. W., Suyu S. H., Koopmans L. V. E., Bolton A. S., 2012, *ApJ*, 752, 163  
 Sonnenfeld A. et al., 2018, *PASJ*, 70, S29  
 Stark D. P. et al., 2013, *MNRAS*, 436, 1040  
 Suyu S. H., Marshall P. J., Auger M. W., Hilbert S., Blandford R. D., Koopmans L. V. E., Fassnacht C. D., Treu T., 2010, *ApJ*, 711, 201  
 Swinbank A. M. et al., 2009, *MNRAS*, 400, 1121  
 Tanaka M. et al., 2016, *ApJ*, 826, L19  
 Tanaka M. et al., 2018, *PASJ*, 70, S9  
 Treu T., Auger M. W., Koopmans L. V. E., Gavazzi R., Marshall P. J., Bolton A. S., 2010, *ApJ*, 709, 1195  
 Tyson J. A., Valdes F., Wenk R. A., 1990, *ApJ*, 349, L1  
 van Dokkum P. G., 2001, *PASP*, 113, 1420  
 Vegetti S., Czoske O., Koopmans L. V. E., 2010a, *MNRAS*, 407, 225  
 Vegetti S., Koopmans L. V. E., Bolton A., Treu T., Gavazzi R., 2010b, *MNRAS*, 408, 1969  
 Verdugo T. et al., 2014, *A&A*, 571, A65  
 Vernet J. et al., 2011, *A&A*, 536, A105

- Wen Z. L., Han J. L., Liu F. S., 2012, *ApJS*, 199, 34  
 Wong K. C. et al., 2018, *ApJ*, 867, 107  
 Wong K. C. et al., 2019, preprint ([arXiv:1907.04869](https://arxiv.org/abs/1907.04869))  
 York D. G. et al., 2000, *AJ*, 120, 1579  
 Zitrin A., Broadhurst T., 2009, *ApJ*, 703, L132

## APPENDIX A: ADDITIONAL SERENDIPITOUS LENS CANDIDATES FROM THE HSC-SSP S18A

During our visual inspection of galaxy groups and clusters, some galaxy-scale lenses were discovered serendipitously, which happen

to be either member galaxies of the group or field galaxies in the vicinity. Since the lensing is due to an individual galaxy rather than a group/cluster (e.g. see the right most panel of Fig. 2), these systems are excluded from our formal SuGOHI-c sample and are reported here instead.

**Table A1.** Lens candidate statistics for SuGOHI-g, similar with Table 2.

	Grade			Total	Previously known / spectroscopically confirmed
	A	B	C		
SuGOHI-g	6	35	90	131	15
CAM	1	5	32	38	3
F	2	4	13	19	7
R	0	5	11	16	3
W	0	8	14	22	4
Serendipity	4	20	38	62	3

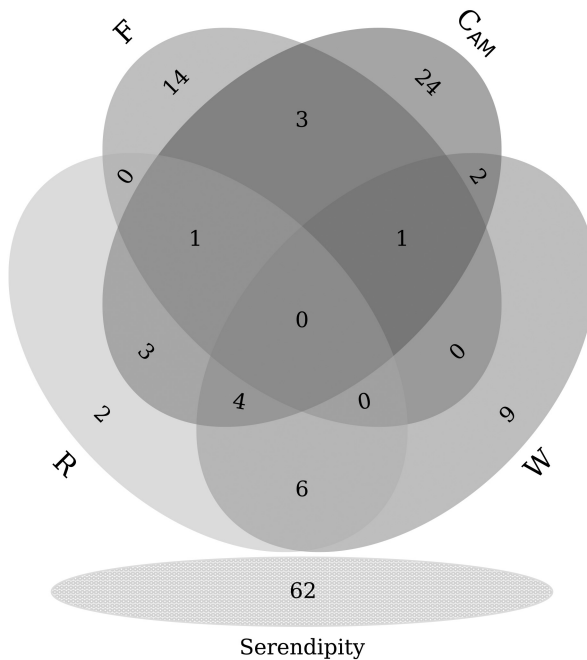


**Figure A1.** Similar to Fig. 3, the distribution of lens candidates at galaxy scales according to the parent cluster catalogues with  $R_{\text{arc}} < 2$  arcsec. The Venn diagram is divided into two panels: 69 lens systems of SuGOHI-g correspond to the parent cluster (upper) and 62 lens systems, which are serendipitously (bottom) discovered during the inspection.

**Table A2.** Extra lens candidates at galaxy scales discovered serendipitously.

Name	$\alpha$ (J2000)	$\delta$ (J2000)	$z_{\ell, \text{phot}}$	$z_{\ell, \text{spec}}$	$R_{\text{arc}}$ (arcsec)	Rank	$\sigma_{\text{Rank}}$	Grade	PC	References
HSC J0154–0039	28.6032	−0.6610	0.18	...	1.31	1.89	0.74	B	...	...
HSC J0157–0500	29.3327	−5.0109	0.28	...	1.32	2.22	0.42	B	CAMRW	...
HSC J0208–0433 <sup>D</sup>	32.1339	−4.5544	0.75	...	1.46	1.89	0.60	B	F	8
HSC J0209–0244	32.4809	−2.7451	0.56	...	1.10	3.00	0.00	A	...	...
HSC J0214–0405 <sup>K</sup>	33.5467	−4.0842	0.65	0.609	1.90	3.00	0.00	A	F	7, 9
HSC J0217–0513 <sup>K</sup>	34.4048	−5.2249	0.64	0.646	1.71	3.00	0.00	A	CAMF	3, 9
HSC J0218–0159	34.5994	−1.9844	0.28	...	1.82	1.75	0.71	B	CAMW	...
HSC J0218–0539	34.5983	−5.6558	0.67	0.691	1.92	1.56	0.68	B	F	...
HSC J0228–0617	37.1722	−6.2915	0.73	...	1.87	1.57	0.50	B	CAMF	...
HSC J0233–0205	38.3446	−2.0920	0.49	...	1.68	2.71	0.45	A	...	...
HSC J0839+0210	129.8766	2.1733	0.67	...	1.91	1.56	0.68	B	...	...
HSC J0904–0102 <sup>K</sup>	136.1239	−1.0412	0.82	0.957	1.33	3.00	0.00	A	...	20
HSC J0913+0039† <sup>D</sup>	138.3797	0.6516	0.37	0.409	1.73	1.56	0.96	B	...	4, 5
HSC J0923+0213	140.7907	2.2308	1.05	...	1.10	2.00	0.50	B	...	...
HSC J0925+0017	141.4375	0.2841	0.85	...	1.81	2.22	0.67	B	...	...
HSC J0959+0234	149.8789	2.5743	1.13	...	1.01	1.78	0.63	B	...	...
HSC J1143+0040	175.8242	0.6760	0.36	...	1.71	1.67	0.47	B	...	...
HSC J1201–0012 <sup>D</sup>	180.4162	−0.2073	0.25	...	1.89	1.56	0.50	B	R	4
HSC J1222+0205† <sup>D</sup>	185.6720	2.0995	0.24	0.229	1.85	1.75	0.71	B	RW	4
HSC J1234–0009 <sup>D</sup>	188.5910	−0.1573	0.41	...	1.69	1.89	0.31	B	CAM	4
HSC J1344–0020	206.2318	−0.3376	0.42	...	1.76	1.56	0.50	B	...	...
HSC J1405–0028	211.2849	−0.4751	0.56	...	1.78	1.63	0.52	B	RW	...
HSC J1410–0109	212.7040	−1.1630	0.66	...	1.07	2.44	0.73	B	...	...
HSC J1413–0133	213.4980	−1.5600	0.96	...	1.51	1.56	0.68	B	...	...
HSC J1418–0003	214.7199	−0.0660	0.55	...	1.46	1.89	0.60	B	...	...
HSC J1420+0059	215.0560	0.9905	0.96	...	1.45	1.78	0.67	B	...	...
HSC J1421+0012	215.3635	0.2015	0.55	...	1.30	1.89	0.57	B	...	...
HSC J1443–0007	220.9792	−0.1252	0.89	...	1.29	2.11	0.31	B	...	...
HSC J1501+4221	225.3007	42.3538	0.27	...	1.30	2.78	0.42	A	...	...
HSC J1544+4427	236.2224	44.4637	0.66	...	0.94	1.67	0.47	B	...	...
HSC J1608+4200	242.0651	42.0026	0.64	0.615	1.85	1.56	0.50	B	W	...
HSC J1613+5406	243.4006	54.1154	1.13	0.766	1.29	2.33	0.67	B	...	...
HSC J1618+5449	244.6470	54.8230	0.81	...	1.60	1.56	0.68	B	CAM	...
HSC J1640+4214	250.0049	42.2439	0.66	...	1.97	1.56	0.50	B	...	...
HSC J2208+0446†	332.0220	4.7676	0.27	...	1.60	1.56	0.50	B	W	...
HSC J2212–0018	333.0950	−0.3032	0.91	...	1.31	2.00	0.50	B	F	...
HSC J2236+0240	339.2255	2.6785	0.38	...	1.14	1.67	0.82	B	...	...
HSC J2310+0247 <sup>D</sup>	347.5196	2.7999	0.37	0.390	1.75	1.56	0.68	B	RW	6
HSC J2323–0030 <sup>D</sup>	350.9419	−0.5105	0.91	...	1.53	2.33	0.67	B	...	3
HSC J2324+0127†	351.0397	1.4579	0.19	0.190	1.94	2.44	0.83	B	W	...
HSC J2331+0000	352.7770	0.0035	0.69	...	1.10	2.00	0.71	B	...	...

Note. References: <sup>3</sup>Jacobs et al. (2019), <sup>4</sup>Petrillo et al. (2019), <sup>5</sup>Sonnenfeld et al. (2018), <sup>6</sup>Wong et al. (2018), <sup>7</sup>More et al. (2012), <sup>8</sup>More et al. (2016), <sup>9</sup>Cabanac et al. (2007), <sup>20</sup>Jaelani et al. (2020).

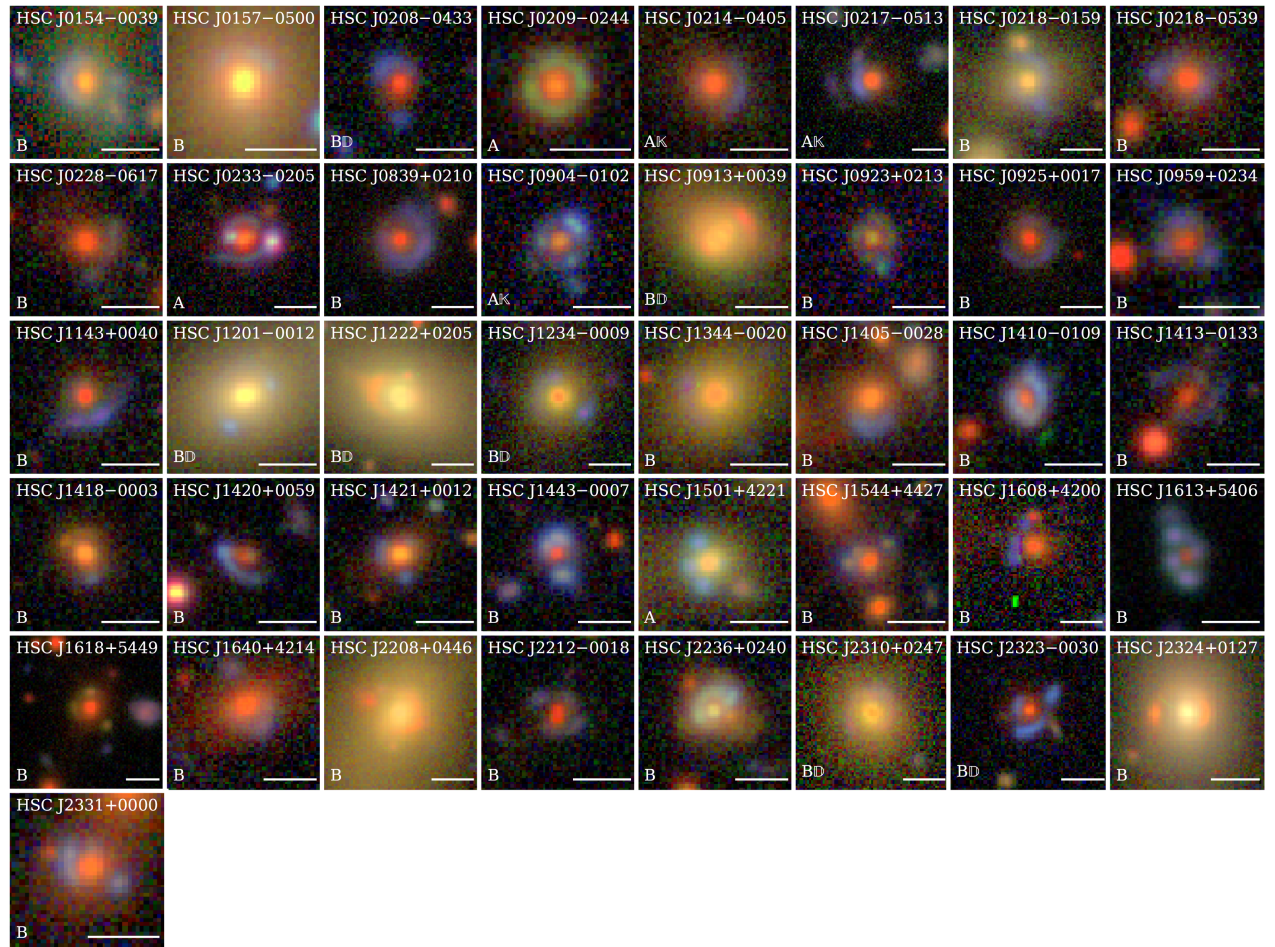


**Figure A2.** Lens candidates at galaxy scales with grades A and B (labels shown on the bottom left). Spectroscopically confirmed, previously discovered, or known lenses are indicated by 'C,' 'D,' or 'K,' respectively. All images are oriented with north up and east left. Scale bars corresponding to 3 arcsec are displayed in the bottom right corner. The grade C candidates from this sample are made available on the same page as the formal SuGOHI-c sample (<http://www-utap.phys.s.u-tokyo.ac.jp/~oguri/sugohi/>).

<sup>1</sup>Department of Physics, Kindai University, 3-4-1 Kowakae, Higashi-Osaka, Osaka 577-8502, Japan

<sup>2</sup>Astronomical Institute, Tohoku University, 6-3 Aramaki, Aoba-ku, Sendai 980-8578, Japan

<sup>3</sup>Astronomy Study Program and Bosscha Observatory, FMIPA, Institut Teknologi Bandung, Jl. Ganesha 10, Bandung 40132, Indonesia

<sup>4</sup>Kavli Institute for the Physics and Mathematics of the Universe (IPMU), 5-1-5 Kashiwanoha, Kashiwa-shi, Chiba 277-8583, Japan

<sup>5</sup>The Inter-University Centre for Astronomy and Astrophysics (IUCAA), Post Bag 4, Ganeshkhind, Pune 411007, India

<sup>6</sup>Department of Physics, The University of Tokyo, 7-3-1 Hongo, Bunkyo-ku, Tokyo 113-0033, Japan

<sup>7</sup>Research centre for the Early Universe (RESCEU), The University of Tokyo, 7-3-1 Hongo, Bunkyo-ku, Tokyo 113-0033, Japan

<sup>8</sup>Leiden Observatory, Leiden University, Niels Bohrweg 2, NL-2333 CA Leiden, the Netherlands

<sup>9</sup>Max-Planck-Institut für Astrophysik, Karl-Schwarzschild-Straße 1, D-85748 Garching, Germany

<sup>10</sup>Physik-Department, Technische Universität München, James-Franck-Straße 1, D-85748 Garching, Germany

<sup>11</sup>Academia Sinica Institute of Astronomy and Astrophysics (ASIAA), 11F of ASMAB, No. 1, Section 4, Roosevelt Road, Taipei 10617, Taiwan

<sup>12</sup>Subaru Telescope, National Astronomical Observatory of Japan, 2-21-1 Osawa, Mitaka, Tokyo 181-0015, Japan

<sup>13</sup>Laboratory of Astrophysique, École Polytechnique Fédérale de Lausanne (EPFL), Observatoire de Sauverny, CH-1290 Versoix, Switzerland

<sup>14</sup>Department of Liberal Arts, Tokyo University of Technology, 5-23-22 Nishikamata, Ota-ku, Tokyo 144-8650, Japan

<sup>15</sup>National Optical Astronomy Observatory, 950 N Cherry Avenue, Tucson, AZ 85719, USA

<sup>16</sup>Department of Astronomy, University of Geneva, ch. d'Écogia 16, CH-1290 Versoix, Switzerland

<sup>17</sup>Department of Astrophysics and Atmospheric Sciences, Kyoto Sangyo University, Kyoto, Kyoto 603-8555, Japan

This paper has been typeset from a  $\text{\TeX}$ / $\text{\LaTeX}$  file prepared by the author.